

UNCLASSIFIED

AD 258 436

*Reproduced
by the*

**ARMED SERVICES TECHNICAL INFORMATION AGENCY
ARLINGTON HALL STATION
ARLINGTON 12, VIRGINIA**



UNCLASSIFIED

NOTICE: When government or other drawings, specifications or other data are used for any purpose other than in connection with a definitely related government procurement operation, the U. S. Government thereby incurs no responsibility, nor any obligation whatsoever; and the fact that the Government may have formulated, furnished, or in any way supplied the said drawings, specifications, or other data is not to be regarded by implication or otherwise as in any manner licensing the holder or any other person or corporation, or conveying any rights or permission to manufacture, use or sell any patented invention that may in any way be related thereto.

CORNELL AERONAUTICAL LABORATORY,

AD 258436

REPORT NO. AF-1270-A-2

AN INVESTIGATION OF LAMINAR HEAT TRANSFER
TO SLENDER CONES IN THE HYPERSONIC SHOCK TUNNEL

by
Charles E. Wittliff
and
Merle R. Wilson
May 1961

Contract No. AF 33(616)-6025

XEROX

4660

B U F F A L O , N E W Y O R K

WADD TN 59-6

AN INVESTIGATION OF LAMINAR HEAT TRANSFER
TO SLENDER CONES IN THE HYPERSONIC SHOCK TUNNEL

Charles E. Wittliff
Merle R. Wilson

CORNELL AERONAUTICAL LABORATORY, INC.
Buffalo, New York

Report No. AF-1270-A-2

May 1961

Contract No. AF-33(616)-6025

Project No. 7064
Task No. 70169

Aeronautical Research Laboratory
AIR FORCE RESEARCH DIVISION
AIR RESEARCH AND DEVELOPMENT COMMAND
UNITED STATES AIR FORCE
Wright-Patterson Air Force Base

FOREWORD

The study on which this report is based constitutes a part of a research program on aero-thermo characteristics of flight of hypersonic vehicles. This program is sponsored by the U. S. Air Force under Contract AF.33(616)-6025, Project No. 7064 "Thermo-Aerodynamic Characteristics at Hypersonic Mach Numbers", Task No. 70169 "Research on Aerodynamic Flow Fields". The project is administered by the Aeronautical Research Laboratory of the Air Force Research Division with Mr. Robert D. Stewart as Task Scientist.

The authors wish to acknowledge the assistance and cooperation rendered them by their colleagues in the Aerodynamic Research Department, particularly Dr. H. K. Cheng for the consultations regarding his theoretical analysis. Special thanks are also due Miss Eileen Stager who performed the data reduction and numerical calculations.

In addition, the authors thank the McDonnell Aircraft Co. for the use of the cone model during the investigation. The model was originally constructed by the Experimental Facilities Division of C. A. L. for McDonnell.

ABSTRACT

As part of a general study of the aero-thermo-characteristics of flight of hypersonic vehicles, an investigation of laminar heat transfer to slender yawed cones has been conducted at the Cornell Aeronautical Laboratory, Inc. In this study, experiments have been made in the CAL 11 by 15-inch shock tunnel at Mach numbers from 11 to 13 and at yaw angles up to 14 degrees. Both sharp and blunt-nose cones having a 5-degree half angle were tested.

The heat-transfer rates are compared with theoretical predictions. The effects on the local heat-transfer rates of the boundary-layer displacement thickness, transverse curvature, yaw, nose bluntness, and the entropy sublayer are discussed. It is shown that, at zero yaw, the experimental data for the sharp cone are in good agreement with theory when boundary-layer displacement and transverse-curvature effects are included. For the yawed sharp cone, the heat-transfer rates along the most windward streamline are in good agreement with E. Reshotko's theory for yaw angles up to 3 degrees. At larger yaw angles, the experimental heat transfer was found to be greater than that predicted theoretically. However, at these yaw angles the heat-transfer distribution on the windward side was in good agreement with laminar boundary-layer calculations based on an assumption of local similarity. The zero-yaw tests of the blunted cones showed qualitative agreement with H. K. Cheng's shock-layer theory for slender blunt-nose bodies.

TABLE OF CONTENTS

FOREWORD	ii
ABSTRACT	iii
LIST OF ILLUSTRATIONS	v
LIST OF TABLES	v
LIST OF SYMBOLS	vi
INTRODUCTION	1
THEORETICAL FLOW ABOUT CONES	2
Pointed Cone at Zero Yaw Without Interaction	3
Boundary-Layer Displacement Effect	4
Transverse-Curvature Effect	5
Slip Flow Effects	7
Inviscid Flow About a Yawed Cone	8
Laminar Heat Transfer to a Yawed Cone	9
Nose Bluntness Effects	10
DESCRIPTION OF THE EXPERIMENTS	11
Shock Tunnel and Test Conditions	11
Models and Instrumentation	16
Schlieren Apparatus	18
RESULTS AND DISCUSSION	19
Sharp Cone at Zero Yaw	19
Heat Transfer Along the Most Windward Streamline at a Yawed Cone	22
Circumferential Heat Transfer Distribution at Large Yaw Angles	23
Blunt-Nose Cone Experiments at Zero Yaw	26
CONCLUSIONS	28
REFERENCES	31
APPENDIX A - Boundary-Layer Displacement Effect on Cones	37
APPENDIX B - Determination of Flow Angularity From Circumferential Heat Transfer Distributions	40

LIST OF ILLUSTRATIONS

<u>Figure</u>		<u>Page</u>
1	CAL 11-by 15-inch Hypersonic Shock Tunnel	47
2	Variation of Mach Number with Nozzle Stagnation Pressure	48
3	Typical Calibration Results for Mach Number (M) Survey	49
4	Typical Drum-Camera Oscilloscope Record	50
5a	Photograph of Sharp 5° Half-Angle Cone	51
5b	Sketch of 5° Half-Angle Cone Showing Location of Heat Transfer Elements	51
6	Photograph of Blunted 5° Half-Angle Cone - D = 0.1925 in.	52
7	15° Wedge Nozzle Used for Tests	53
8	Heat Transfer to a Pointed Cone at Zero Yaw and Laminar Theory	54
9	Ratio of Heat Transfer Along Most Windward Streamline to Zero Yaw Heat Transfer - 5° Half-Angle Cone at M = 12, $T_{STAG} = 2000^{\circ}\text{K}$	55
10a	Circumferential Heat Transfer Distribution - 4.5° Yaw	56
10b	Circumferential Heat Transfer Distribution - 9.5° Yaw	56
10c	Circumferential Heat Transfer Distribution - 13.7° Yaw	56
11	Heat Transfer to a Blunt 5° Half-Angle Cone at Zero Yaw	57
12	Schlieren Photograph of Flow About Blunt 5° Half-Angle Cone at Zero Yaw	58
13	Shock Wave Shape for a Blunt 5° Half-Angle Cone at Zero Yaw	59
14a	Circumferential Heat Transfer Distribution - Run 523	60
14b	Circumferential Heat Transfer Distribution - Run 525	60
14c	Circumferential Heat Transfer Distribution - Run 528	60

LIST OF TABLES

Table

I	Flow Conditions for Pointed Cone Zero Yaw Tests	44
II	Flow Conditions for Yawed Pointed Cone Tests	44
III	Flow Conditions for Blunted Cone Zero Yaw Tests	45
IV	x/D Positions of Instrumented Stations for Blunted Cones	46

LIST OF SYMBOLS

$C =$	$\frac{\mu_w/\mu_c}{T_w/T_c}$, Chapman-Rubesin viscosity coefficient
c	specific heat of Pyrex glass
$C_H =$	$g/\rho_\infty U_\infty (H_{aw} - H_w)$, heat transfer parameter
D	nose diameter
$d_c =$	$\frac{0.968}{M_c^2} \frac{T_w}{T_c} + 0.145(\gamma-1)$, parameter in boundary-layer displacement analysis, Ref. 7
$F_r(K)$	parameter in boundary-layer displacement analysis, Ref. 7
H	enthalpy
$K =$	$M_\infty \Theta_c$, hypersonic similarity parameter
κ	thermal conductivity of Pyrex glass, also nose-drag coefficient, Ref. 32
M	Mach number
p	pressure
Pr	Prandtl number
q	heat transfer rate
r	body radius
Re	Reynolds number
St	Stanton number
T	temperature
U	velocity
X	axial distance
y	normal distance
α	angle of attack or angle-of-attack component of flow angularity

β	yaw component of flow angularity
γ	specific heat ratio
Δ	parameter proportional to δ^* in transverse-curvature analysis, Ref. 10
δ	boundary-layer thickness
δ^*	boundary-layer displacement thickness
$\epsilon =$	$\frac{\gamma-1}{\gamma+1}$, parameter in blunt-cone analysis, Ref. 32
η	compressible laminar boundary-layer similarity parameter, Refs. 7, 10
θ_c	cone half-angle
θ_s	conical shock-wave angle
μ	viscosity coefficient
ρ	density
$\bar{\chi} =$	$M^3/\sqrt{C/Re}$, hypersonic viscous interaction parameter
ψ	yaw angle
ω	circumferential angle measured from most-windward streamline

Subscripts

aw	adiabatic wall conditions
C	conditions at outer edge of boundary layer on cone
D	nose diameter taken as reference length
o	free-stream stagnation conditions, or conditions along most-windward streamline
w	conditions at wall or cone surface

X axial distance taken as reference length
 l first-order term in yawed cone analysis
 ∞ free-stream conditions

INTRODUCTION

In recent years there has developed an increasing interest in hypersonic flight at high altitudes with maneuverable vehicles. Vehicles capable of sustained flight at hypersonic speeds within the earth's atmosphere will undoubtedly generate aerodynamic lift while maintaining low drag. This implies slender shapes flying at an angle of attack. They will presumably have local bluntness at the nose and leading edges to accommodate the high heat-transfer rates in these regions. Such bodies will experience flow phenomena not generally encountered in supersonic flight at low altitudes, such as boundary-layer displacement, transverse curvature, slip flow and real gas effects. A slender cone will experience most of these hypersonic flow phenomena. In addition, its shape makes it amenable to theoretical solutions for the various phenomena of interest. Consequently, as part of a general study of the aero-thermo-characteristics of flight of hypersonic vehicles, an investigation of laminar heat transfer to a slender cone including yaw and nose-bluntness effects has been conducted at the Cornell Aeronautical Laboratory, Inc.*

In this investigation, experiments with a 5° half-angle cone have been made in the hypersonic shock tunnel at air flow Mach numbers from 11 to 13, and free-stream Reynolds numbers from 2×10^5 to 2×10^6 per foot. A sharp cone was tested at yaw angles up to 14 degrees. For the blunt-nose tests at zero yaw, heat-transfer data were obtained at axial positions in the range $1.75 \leq X/D \leq 112$.

* This work is also reported in IAS Preprint 61-213-1907 (Ref. 1).

An important objective of this study has been to compare the experimental data with theoretical predictions. Also, it has been necessary to use theory to determine the inviscid flow properties outside the boundary layer because no model surface pressures were measured.* Consequently, various inviscid and viscous flow theories have been studied during the present program. In this report, the pertinent hypersonic flow phenomena are discussed and the available theoretical solutions for slender cones are reviewed. Next, the experiments are described. Finally, the heat-transfer results are presented and compared with the various theoretical predictions. The effects on local heat-transfer rates of boundary-layer displacement thickness, transverse curvature, yaw, nose bluntness, and the entropy sublayer are discussed. It will be shown that in some instances the experimental data are in good agreement with theory when those various phenomena are taken into account, whereas in other cases the data and theory disagree considerably.

THEORETICAL FLOW ABOUT CONES

An objective of the present study of laminar heat transfer to slender cones has been to assess the range of accuracy of various theories by comparison with the experimental data. To achieve this goal it has been necessary to review the various inviscid and viscous theories

* At the time this study was undertaken no pressure transducers having the required sensitivity and small size were available. Suitable pressure gauges have since been developed at CAL.

for flow about cones including yaw and nose-bluntness effects. Boundary-layer displacement thickness and transverse-curvature effects were found to be present; consequently, they had to be accounted for in theoretical calculations in order to obtain good agreement with the experimental data. Also, theoretical methods have been used to calculate the inviscid flow conditions at the outer edge of the boundary layer because no surface pressure measurements were made during the experiments.

The more important features of the flow phenomena and the pertinent theoretical results will be described here before discussing the present experiments. Additional details regarding the interaction of the boundary layer and the inviscid flow are presented in Appendix A.

POINTED CONE AT ZERO YAW WITHOUT INTERACTION

The inviscid supersonic flow field about a pointed, right circular cone at zero yaw can be treated by the theory of Taylor and MacColl². Numerical solutions according to this theory have been tabulated by Kopal³ and Sims⁴ for an ideal gas. Kopal's tabulated results³ have been used to obtain the local flow conditions at zero yaw because no real gas effects were present in the inviscid flow for the conditions of the present experiments.

The laminar boundary layer on a cone has been studied for many years, and a review of the various theoretical solutions may be found in References 5 and 6. The general results of these solutions for the laminar heat transfer to a pointed cone at zero yaw and constant surface pressure is

$$St = 0.3321 \sqrt{3} R_w^{-\frac{1}{3}} \sqrt{(C/Re_x)_c} \quad (1)$$

where the Stanton number, Prandtl number, Reynolds number, and Chapman-Rubesin viscosity constant are defined in the List of Symbols.

The heat-transfer rates obtained from Eq. (1) apply only for cone flow where the boundary-layer thickness is small compared to the body radius. Under these circumstances, the boundary-layer displacement thickness is small and the Mangler transformation (the $\sqrt{3}$ factor in Eq. (1)) is sufficient for describing the transverse-curvature effect. However, the displacement thickness and transverse-curvature effects were found to be evident in the present experiments and had to be included in the theoretical calculation.

BOUNDARY-LAYER DISPLACEMENT EFFECT

The boundary-layer displacement effect results from the growth of a relatively thick boundary layer which produces an outward deflection of the stream surfaces. This deflection can be sufficiently large to change the "effective" shape of the body and perturb the inviscid conical flow field. The perturbation in the inviscid conical flow results in "induced" pressure changes on the body which, in turn, affects the growth of the viscous boundary layer. The solution obtained by Probstein⁷ is used in the present work to account for this effect.*

Probstein has represented the induced-pressure distribution by a Taylor series expansion and has evaluated the coefficients, which have the form $d(p/p_\infty)/d\theta$ and $d^2(p/p_\infty)/d\theta^2$, by applying the tangent-cone approximation and utilizing Lees' hypersonic approximation⁸.

Having determined the induced pressure as a function of the interaction

* Additional details of the theory are given in Appendix A.

parameter. $\bar{\chi}_c = M_c^3 / \gamma (C/Re_x)_c$, the velocity and temperature profiles are expanded in a series in $\bar{\chi}_c$ and substituted into the laminar boundary-layer equations. The zero-order solution corresponds to the Mangler transformation for the zero-pressure-gradient boundary layer on a cone. The first-order correction to the heat transfer is, for $Pr = 1$,

$$\frac{g - g_0}{g_0} = \left[-0.350 + 0.111 \frac{T_w}{T_c} + (0.429\gamma - 0.028) M_c^2 \right] \frac{d_c F_1(K) \bar{\chi}_c}{\gamma M_c^2} \quad (2)$$

where the zero subscript represents the values obtained for the laminar boundary layer on a cone with zero pressure gradient.

TRANSVERSE-CURVATURE EFFECT

The viscous transverse-curvature effect results from the fact that the boundary layer on an axisymmetric body not only grows in thickness with distance along the surface, but also spreads circumferentially as it grows. The Mangler transformation⁹ provides a direct transformation of the compressible boundary-layer equations for axisymmetric flow to those of a two-dimensional flow when the gas is perfect with constant specific heats and the boundary-layer thickness is small compared to the body radius. Probstein and Elliot¹⁰ have studied the more general problem where the boundary-layer thickness is not necessarily small compared to the body radius.

Probstein and Elliot show that the transverse-curvature effect is characterized by the parameter Δ/r which is essentially the ratio of the displacement thickness to the body radius. They formulate the problem in terms of the compressible "similarity" parameter $\eta \sim y/\sqrt{x}$ and a parameter $\xi \sim \Delta/r$. The stream function and temperature dis-

tribution within the boundary layer are expanded in an asymptotic series in powers of ξ , where the coefficients are functions of γ alone.

They have obtained numerical solutions for the case of the cone with zero pressure gradient for a perfect gas having constant specific heats and a Prandtl number of unity. The first-order corrections have been obtained, where the Mangler transformation represents the zero-order solution. The numerical integration of the boundary-layer equations results in the following first-order correction for the heat-transfer rate for $Pr = 1$

$$\frac{q - q_0}{q_0} = \left[0.517 + 0.913 \frac{T_w}{T_c} + 0.121(\gamma - 1) M_c^2 \right] \frac{\sqrt{(C/Re_x)_c}}{\sqrt{3} \tan \theta_c} \quad (3)$$

where q_0 is the heat-transfer rate obtained using the Mangler transformation.

Probstein⁷ has noted that the corrections for the boundary-layer displacement effect (Eq. (2)) and the transverse-curvature effect (Eq. (3)) and the asymptotic expansion for the flow over a cone are all in inverse powers of $Re_x^{-1/2}$. The principle of linear superposition applies, and the corrections for these effects are directly additive. Consequently, by combining Eqs. (1), (2), and (3), the total heat transfer can be expressed as

$$St = \frac{q}{\rho_c U_c (H_{aw} - H_w)} = 0.3321 \sqrt{3} Pr^{-1/3} \sqrt{(C/Re_x)_c} \left\{ 1 + \left[-0.350 + 0.111 \frac{T_w}{T_c} + (0.429\gamma - 0.028) M_c^2 \right] \frac{d_c F_c(K) \bar{X}_c}{\gamma M_c^2} \right. \\ \left. \left[0.517 + 0.913 \frac{T_w}{T_c} + 0.121(\gamma - 1) M_c^2 \right] \frac{\sqrt{(C/Re_x)_c}}{\sqrt{3} \tan \theta_c} \right\} \quad (4)$$

The experimental data will be compared with theoretical predictions based on this equation for the tests of the pointed cone at zero yaw.

SLIP FLOW EFFECTS

Another point of interest to the present program is the matter of slip flow. The slip flow regime has been somewhat arbitrarily defined^{11, 12}, on the basis of experimental evidence, by the limitations

$$0.01 < \frac{M}{\sqrt{Re}} < 0.1, \quad Re > 1$$

Thus, at Mach numbers near 10, slip flow would be encountered for Reynolds numbers between 10^4 and 10^6 according to this criterion. Since the present experiments extend down to a Reynolds number of 8.4×10^4 , one would expect slip flow effects to be present. However, Hayes and Probstein¹³, on the basis of an order of magnitude analysis, conclude that slip will not be important in affecting skin friction and heat transfer on a slender body, particularly if the body is cool, when

$$\frac{\rho_\infty M_\infty}{\rho_s \sin^3 \theta_s Re_{x_\infty}} \ll 1$$

where θ_s is the shock wave angle. For the present tests at the lowest Reynolds number

$$\frac{\rho_\infty M_\infty}{\rho_s \sin^3 \theta_s Re_{x_\infty}} \approx 0.04$$

and slip effects would not be present according to Hayes and Probstein's criterion.

Thus, the present experiments may help to substantiate one criterion or the other in view of their contradictory predictions of the presence of slip flow effects.

INVISCID FLOW ABOUT A YAWED CONE

Solutions for the inviscid supersonic flow about a yawed pointed cone has been developed by Stone^{14, 15, 16} by first- and second-order perturbations of the Taylor-Maccoll theory. Extensive numerical calculations of Stone's solutions have been published by Kopal^{17, 18}. However, these calculations are inconvenient to use because they are tabulated in a wind-fixed coordinate system. A procedure for converting to body-fixed coordinates is given by Roberts and Riley¹⁹. Recently, calculations of Stone's first-order solution for small angles of attack have been published by Sims²⁰.

Ferri²¹ has shown that Stone's theory does not give the proper entropy distribution at the cone surface. To obtain the correct entropy distribution, he has introduced the concept of a vortical layer of negligible thickness across which the entropy and velocity change discontinuously and the pressure is constant.* Using this concept, Ferri gave a method for correcting the first-order Stone solution. Recently, Willett²³ has developed the second-order vortical-layer corrections.

It should be noted that the existence of the vortical layer does not affect the cone surface pressure or, hence, the forces. On the other hand,

* It is interesting to note that H. K. Cheng has developed²² a hypersonic shock-layer theory for the inviscid flow about a yawed cone which shows the existence of a vortical sublayer. He has obtained a uniformly valid first-order solution which yields an explicit description of the structure of the shock layer and exhibits a vortical sublayer near the cone surface.

the skin friction and heat transfer may be influenced by the presence of the vortical layer. For the present study, the circumferential heat-transfer distribution for large yaw has been computed with and without vortical-layer corrections to the inviscid flow.

LAMINAR HEAT TRANSFER TO A YAWED CONE

The laminar boundary-layer equations for a yawed, pointed cone were first formulated by Moore²⁴. He has obtained a linearized solution for small angles of attack²⁵ and a solution in the plane of symmetry for large angles of attack²⁶. Both of these solutions are for insulated surfaces and do not include heat transfer. Reshotko²⁷ reports that G. M. Low of the NASA (then NACA) Lewis Laboratory has extended Moore's linearized analysis for small angle of attack to include heat transfer. Low's analysis, which has not been published, showed large changes in heat transfer with angle of attack, and also, that there is a significant effect of surface temperature level on the magnitude of this angle-of-attack effect. In Reference 27, Reshotko extends Moore's large angle-of-attack analysis to include heat transfer effects.* The analysis is restricted to the windward streamline in the plane of symmetry (the "most-windward streamline").

In his study of the laminar boundary layer with heat transfer, Reshotko has solved the boundary-layer equations numerically for a range

* An approximate method for calculating the laminar boundary layer with heat transfer on a cone at large angle of attack has been developed by Brunk²⁸ for a Prandtl number of unity.

of wall-to-stagnation temperature ratios and a range of circumferential-velocity gradients. His results have been extrapolated to the higher free-stream Mach numbers of the present tests, and the ratio of the heat transfer along the most windward streamline to the zero-yaw heat transfer has been calculated for yaw angles up to 8 degrees.

Reference 27 also gives a procedure for calculating heat transfer along the most windward streamline of a slender cone at very large yaw angles. This procedure applies the yawed-cylinder results of Reshotko and Beckwith²⁹ and has been used to calculate the heat transfer for yaw angles above 5 degrees in the present study. Both second-order Stone theory¹⁵ as tabulated by Kopal¹⁸ and Newtonian theory³⁰ have been used to calculate the pressure.

NOSE-BLUNTNESSEFFECTS

The inviscid flow about a blunt-nosed cone is a mixture of subsonic flow at the nose and supersonic flow along the cone. The effects of the strong, detached shock wave are felt many nose diameters downstream on the cone influencing both the inviscid flow and the boundary layer. A numerical solution for the supersonic portion of the flow can be obtained by the method of characteristics if the shape of the sonic line between the body and the shock wave, the flow conditions along the sonic line, and the shock-wave shape are known. Even if this information is available, the method of characteristics for axisymmetric bodies is very time-consuming unless a high-speed computer is utilized. This has led to the development of various approximate theories that may be classified as

blast-wave, shock-layer, Newtonian or hypersonic small disturbance.

Hayes and Probstein have given a good review of these theories³¹.

The particular problem of hypersonic flow about a blunt-nosed slender cone has been studied by Cheng³², Chernyi³³ and Lunev³⁴. The latter two authors utilize blast-wave theory (see, for example, Reference 35), whereas Cheng's approach is based on the concept of a thin shock layer. In the present study, the experimental heat-transfer rate and measured shock-wave shapes are compared with Cheng's theory.

Cheng has obtained a complete zero-order solution ($\gamma \rightarrow 1$) for a slender blunt cone at zero yaw. The pressure distribution decreases from the high pressure behind the detached shock to a minimum value less than the pressure on a sharp cone of the same apex, then increases to a level greater than that on the sharp cone, and finally undergoes an oscillatory decay to the pressure on an equivalent sharp cone. The oscillatory decay is probably associated with the zero-order nature of the solution and may not have any physical significance. Cheng has calculated the heat-transfer coefficient on the basis of local similarity for the laminar boundary layer. This displays a behavior similar to that of the pressure distribution. The experimental results are compared with this theoretical solution.

DESCRIPTION OF THE EXPERIMENTS

SHOCK TUNNEL AND TEST CONDITIONS

The experiments were made in the CAL tailored-interface shock tunnel. This facility is discussed in detail in Reference 36, and only a

brief description of the tunnel and its operation will be given here. The CAL 11 by 15 inch hypersonic shock tunnel, Figure 1, consists of a high-pressure driver tube 3.5 inches I. D. by 14 feet long, a driven tube 3 inches I. D. by 14 feet long*, and a three-stage hypersonic nozzle. The first stage of the nozzle is a convergent-divergent contoured nozzle which expands the air to about Mach 4. The second stage is a flow-turning section which serves to deflect the flow through a Prandtl-Meyer expansion and centrifuge diaphragm particles out of the air stream. The third stage is a straight-walled, 15° included-angle nozzle having an 11 by 15 inch test section. Variation of test Mach number can be obtained by varying the entrance area of the third stage expansion; however, all of the present tests were made at a fixed area ratio. A variation in Mach number from 11.3 to 13 occurred as the free-stream Reynolds number was varied from 2×10^5 per foot to 2×10^6 per foot. The duration of useful flow in this configuration is about 2.5 milliseconds following the initial 0.5 to 1 millisecond period required for flow establishment in the nozzle and about the model.

The convergent portion of the first-stage nozzle has an area ratio of 18.9:1. This is sufficient to ensure complete reflection of the incident shock wave and, hence, provide a region of almost stagnant air upstream of the nozzle. The Mach number in this region is less than 0.05 so that

* Prior to the last series of blunt-nose tests ($D = 0.059$ in.), the driven section was lengthened to 28 feet. This served to increase the available testing time.

only negligible errors are introduced in assuming the flow to be stagnant.

As described in Reference 36, tailored-interface operation theoretically occurs at a unique shock-wave Mach number when the specific-heat ratios and speeds of sound of the driver and driven gases are specified. For the present tests helium was used as the driver gas and air as the test gas, both initially at room temperature. This combination will tailor at a shock Mach number of about 4 and a driver-to-driven pressure ratio of about 150. Driver gas pressures from 1000 to 10,000 psia were used in order to vary the Reynolds number.

At a shock Mach number of 4, the temperature of the stagnant air behind the reflected shock wave is about 2000°K. When the air is expanded to Mach 11 to 13 in the test section, the ambient temperature lies between 82°K and 65°K, which is sufficient to avoid oxygen liquefaction. The test flow velocity is about ~~6500~~⁶⁹⁰⁰ ft/sec.

Shock-tube conditions measured in each experiment included initial air pressure in the driven tube, pressure of the driver gas at the time the diaphragm bursts, incident shock-wave speed, and the nozzle reservoir pressure, p_0 , attained behind the reflected shock wave. The nozzle reservoir conditions, including enthalpy, pressure, density, and entropy, are calculated from the measured shock speed and initial air pressure using real-gas, equilibrium flow relations. The measured reservoir pressure provides a check on the calculated reservoir conditions. A complete tabulation of the range of flow conditions for all the tests is presented in Tables I, II, and III.

Calibration studies of the test flow in the 15° wedge nozzle have included simultaneous measurement of static pressures at the tunnel sidewall and pitot pressures across the tunnel using a multiple-probe rake, flow-angularity studies with a multiple-wedge rake instrumented with heat-transfer gauges³⁷, and measurement of surface pressures on a sharp-edged plate at large compressive incidence such that shock wave-boundary-layer interaction effects are negligible. Also, the present heat-transfer measurements on the sharp cone provide further flow angularity data. The static pressures have been measured with a modified Altec-Lansing microphone, Model 21 BR-200-2, and CAL-developed barium titanate piezoelectric transducers. The latter were also used in the pitot-pressure rake.

The average test Mach number varied from 11.3 ± 0.2 at a reservoir pressure of 1000 psia to 13.0 ± 0.1 at 10,000 psia. The fluctuations with time during a single test were about ± 0.2 . Figure 2 shows the measured variation of Mach number with reservoir pressure. The Mach number variation across the test section is shown in Figure 3 for reservoir pressures of 1030 psia and 4350 psia.* At the lower reservoir pressure, the Mach number is essentially constant across the tunnel indicating that the thick boundary layer has produced quite uniform flow in the wedge nozzle. At the higher reservoir pressure, the boundary layer is thinner, and a Mach number gradient exists as would be expected. Measurements

* The size of the available rake necessitated mounting it diagonally in the 11 by 15 inch test section.

of local pitot pressure and flat-plate heat transfer³⁸ at different longitudinal stations on the 15° nozzle centerline have indicated small longitudinal gradients. The maximum Mach number gradient at the test location is estimated to be less than 0.1 per inch.

The flow angularity was previously measured using a wedge rake instrumented for heat-transfer measurement³⁷. The present experiments have produced additional information regarding the flow angularity (Appendix B). The results of these tests indicate the centerline flow at the vertex of the cone to have an angularity of - 0.8 degrees in the pitch plane (downward) and 0.6 degrees in the yaw plane. The negative angularity in the pitch plane can be attributed to boundary-layer growth on the flow-turning wedge in the second stage of the nozzle.

Flow conditions in the test section are calculated from the test Mach number, the reservoir pressure, the stagnation enthalpy, and the entropy assuming isentropic expansion with thermodynamic equilibrium. At the stagnation temperatures and pressures employed, oxygen dissociation is negligible and molecular vibration is the only inert degree of freedom excited. The assumption of a test flow in thermodynamic equilibrium is considered valid on the basis of calculations of typical vibrational relaxation effects to be expected in the first expansion stage of the nozzle.

A typical oscillograph record is shown in Figure 4. The record shows the time histories of the reservoir pressure and the sidewall static pressure as well as a model surface-temperature history and local heat-transfer rate at a typical position on the model.

MODELS AND INSTRUMENTATION

A conical model having a 5° semi-apex angle was tested during the present investigation. Figure 5a shows the cone instrumented with heat-transfer elements axially and circumferentially.* The location of the heat-transfer elements is given in Figure 5b. Note that the elements have their major dimension along a conical ray rather than circumferentially. This was done to minimize the effect of the circumferential variation of heat-transfer rates on this slender cone. The various blunt noses used with this cone had diameters of 0.059, 0.1925, 0.2995 and 0.400 inches. A typical configuration is shown in Figure 6. Note that in this photograph a cylindrical afterbody has been added to the cone. This was done to move the separated wake flow downstream from the last instrumented station. In the early tests the data taken at the last station showed a rather high degree of scatter which was attributed to the nearness of the unsteady separated wake.

The location of the mid-point of the heat-transfer elements in terms of nose diameters is given in Table IV. The tests cover the range from $X/D = 1.75$ to 112, or from very near the nose to well downstream.

The heat-transfer elements shown on the model in Figure 5 are thin-film resistance thermometers of platinum deposited on Pyrex glass sections of the model. A platinum paint is sprayed on the glass and then

* Measurements of the tip bluntness on an optical comparator indicated that the cone had a nose radius of about 0.0001 inches.

the glass pieces are heated in an oven leaving a platinum film about 0.1 micron thick. This technique is described in detail in References 39 and 40.

The heat capacity of such thin-film thermometers is so small that the films record the instantaneous surface temperature history with negligible error. Local heat-transfer rates are obtained by solution of the one-dimensional heat-flux equation with the measured surface-temperature time histories as input data. For most of the tests the solution was obtained numerically using a high-speed computer (IBM-704). During the last group of tests, however, an analogue-computer network which had been under development became available and was utilized so that local heat-transfer rates were recorded directly rather than the surface temperature. The design and operation of this unit is described in Reference 41. The use of this computer network considerably shortens the data reduction process.

Calibration of the models consists of determining the rate of change of resistance with temperature for each heat-transfer element and determining the product ($k\rho c$) of the glass. Pyrex-brand glass is used because of its relative uniformity from sample to sample, and because a value of $\sqrt{k\rho c} = 0.0745 \text{ BTU/ft}^2 \cdot ^\circ\text{F}$ has been established by several procedures. The slope of the resistance-temperature curve is determined from resistance measurements at several temperatures. Over the range of surface temperatures encountered in the experiments, 0 to 50°F, the slope is constant. This calibration is made before and after each series

of tests. The stability of the films is attested to by the fact that the slope rarely changed by more than 2% over a period of six months or more. A few of the films did develop open circuits or attain extremely high resistances; however, this usually happened during the first few runs, indicative of a poorly applied element.

The model was supported by a sting from a circular-arc sector mounted horizontally in the test section. Thus, the model was yawed rather than pitched. This was done because the yaw plane was the plane of symmetry in the wedge nozzle. The angles of attack, yaw, and roll were set to about ± 0.1 degrees relative to the geometric axes of the tunnel.

The position of the model in the test section and its relation to the wedge nozzle is shown in Figure 7. The center of rotation for the yaw tests is about 2.5 inches aft of the cone vertex.

SCHLIEREN APPARATUS

The schlieren system employed was a conventional, off-axis single-pass arrangement with 10-ft. focal length, 16-inch diameter, spherical mirrors. A barium-titanate condenser-discharge spark-light source was used. This light source had a spark duration of about 0.1 microseconds. The spark was triggered by the arrival of the shock wave at the last instrumentation station in the shock tube. A time delay of 2 to 2.5 milliseconds was used to allow the flow to become fully established in the nozzle and about the model.

The shock wave coordinates relative to the model axis were measured from enlargements of the schlieren negatives.

RESULTS AND DISCUSSION

In presenting the experimental results of this study, the zero-yaw tests of the sharp cone are discussed first including the magnitude of the boundary-layer displacement and transverse-curvature effects. Next the effect of yaw on the heat transfer along the most-windward streamline is described. Then the circumferential heat-transfer distribution at large yaw is presented. Finally, the blunt-nose experimental results are discussed. In each case comparison is made with calculations based on the pertinent theories discussed previously.

SHARP CONE AT ZERO YAW

Because of the flow angularity in the test section, none of the tests were made at a true zero yaw. However, the zero geometrical yaw experiments were sufficiently close to true zero yaw that the results can be correlated with zero-yaw theory provided the correct local inviscid flow conditions are used. The implication is that yaw effects, that is cross flow, have negligible influence on the boundary layer.

The first-order theory of Stone¹⁴ tabulated in Reference 17 has been used in the manner described by Roberts and Riley¹⁹ to determine the local inviscid flow conditions. The experimental heat-transfer rates have been reduced to Stanton number based on the local density and velocity and the difference between the local adiabatic-wall enthalpy and the enthalpy at the wall temperature

$$St = \frac{q}{\rho_c U_c (H_{aw} - H_w)}$$

The results are shown as function of Reynolds number based on local flow conditions and axial distance along the cone, $Re = \frac{\rho_c U_c X}{\mu_c}$, in Figure 8 for the 5° half-angle cone. The scatter, which is about $\pm 10\%$, was fairly typical of shock tunnel testing at the time the tests were made.

The theoretical prediction for laminar heat transfer to a cone in the absence of boundary-layer interactions is given by Eq. (1) and is shown in Figure 8. The data are seen to lie, on the average, about 20% above the theoretical curve. Most of this 20% discrepancy can be attributed to boundary-layer displacement and transverse-curvature effects. The theoretical predictions of the laminar heat transfer with boundary-layer interactions have been calculated according to Eq. (4) and are shown also in Figure 8. At the lowest free-stream Reynolds number ($2.4 \times 10^5/\text{ft}$), the data and the theory agree quite well. At $Re_\infty = 9.0 \times 10^5/\text{ft}$, the data lie about 10% above the theory at the most-forward instrumented station ($X = 3.0 \text{ in.}$), are within 10% at the second station ($X = 5.1 \text{ in.}$), and scatter about the theory at the aft station ($X = 6.6 \text{ in.}$). At the highest free-stream Reynolds number ($Re_\infty = 17.4 \times 10^5/\text{ft}$), the data lie from 10% to 40% above the theory at the first station ($X = 3.0 \text{ in.}$) and within 10% of the theory at the aft station.

Two things are noted about the data relative to the theory: (1) the variation of the data with Reynolds number for a given run is slightly greater than predicted by the theory; (2) the deviation of the data from the theory increases as the Reynolds number is increased. In fact, at the highest free-stream Reynolds number, the theoretical corrections for

boundary-layer displacement and transverse-curvature effects account for only one-half of the deviation of the data from laminar boundary-layer theory without interactions. The difference in Reynolds number dependence between data for a given run and theory is most likely a model effect. For example, it is noted that data at corresponding positions on the model for the three runs shown in Figure 8 apparently do vary as $Re_x^{-1/2}$ although they fall at differing levels about the theoretical curve. Such a model effect is probably caused by the flow separation at the base of the cone since the cylindrical afterbody had not yet been installed at the time of these tests. The ability of a wake in hypersonic flow to influence the boundary layer on a model has been observed also in the flat-plate study reported in Reference 42. This may also account for the disagreement between experiment and theory noted in Item (2) since any upstream influence of the wake is certainly Reynolds number dependent.

Eckert's empirical reference-enthalpy method⁴³ has also been used as the basis for calculating laminar boundary-layer heat transfer. These calculations were about 6% higher than the results obtained from Eq. (1). When the boundary-layer displacement and transverse-curvature corrections were added, the method predicted heat-transfer rates that were 6 to 9% greater than the experimental data at the lowest free-stream Reynolds number ($Re_\infty = 2.4 \times 10^5/\text{ft}$), from 7% above to 9% below the data at the intermediate Reynolds number ($Re_\infty = 9.0 \times 10^5/\text{ft}$), and from 0 to 13% below the data at the highest Reynolds number ($Re_\infty = 17.4 \times 10^5/\text{ft}$). Thus this procedure gives better agreement with the data at the two higher free-

stream Reynolds numbers and poorer agreement at the lowest Reynolds number than is obtained using the method based on Eq. (1).

In general, it may be concluded that either procedure gives reasonably good agreement with the data when account is taken of the boundary-layer displacement and transverse-curvature effects. It should be mentioned that uncertainties as to the correct value of the Prandtl number could easily account for larger errors than the discrepancy between theory and data, particularly with Eckert's reference-enthalpy method in which the Prandtl number is evaluated at a temperature considerably higher than the wall temperature.

The close agreement between the experimental data and the theory at the lowest Reynolds number indicates the absence of any noticeable slip-flow effects. This is in agreement with the criterion of Hayes and Probstein¹³ and contradicts that of Tsien^{11, 12}.

HEAT TRANSFER ALONG THE MOST-WINDWARD STREAMLINE OF A YAWED CONE

The heat-transfer rates along the most-windward streamline for the pointed cone at yaw are shown in Figure 9 as the ratio of the experimental rate, q , to the zero-yaw rate, $q_{\alpha=0}$. As was indicated previously, none of the tests were at a true zero yaw because of the flow angularity. Therefore, the value of $q_{\alpha=0}$ was determined by extrapolating to zero the measured heat-transfer rates for the near-zero yaw tests (geometrical yaw equal to 0, $\pm 1^\circ$, $\pm 2^\circ$). The three symbols at each yaw angle represent the three axial stations on the cone.

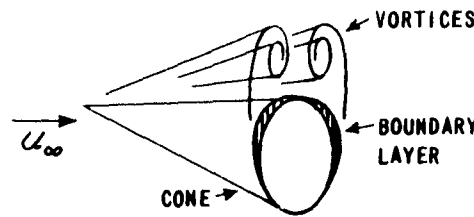
The data are seen to be in very good agreement with Reshotko's theory²⁷ for yaw angles up to 3 degrees. Beyond 3 degrees yaw, the data falls somewhat above the theoretical curve. It should be noted that the calculation of the theoretical curve required graphical extrapolation of some of Reshotko's results to the higher Mach number of the present study. Extrapolation of the results appeared reasonable and was carefully done; however, it does inject some uncertainty into the accuracy of the theoretical curve.

The heat-transfer ratio for large yaw angles (above 5 degrees) has been calculated according to the Reshotko and Beckwith's theory for a yawed cylinder²⁹. This calculation has been made using both second-order Stone theory¹⁸ and Newtonian theory³⁰ to predict the pressures. Both theoretical curves fall noticeably below the experimental data. Again it was necessary to graphically extrapolate Reshotko and Beckwith's results to higher Mach number. However, it is not believed that any error involved in this extrapolation contributed significantly to the disagreement between the data and the theory.

CIRCUMFERENTIAL HEAT-TRANSFER DISTRIBUTION AT LARGE YAW ANGLES

The circumferential heat-transfer distributions at large yaw angles (4.5, 9.5, and 13.7 degrees) are shown in Figure 10 as the ratio of the local heat-transfer rate to the heat-transfer rate along the most-windward streamline. This presentation permits a direct comparison of the data at each of the axial stations. Except for some scattered points, the heat-transfer rate at 4.5 degrees yaw decreases continuously from the most-

windward streamline position. At 9.5 and 13.7 degree yaw, the heat-transfer rates near 180 degrees are higher than those at 150 and 210 degrees. This suggests the formation of a pair of separated vortices resulting from the large cross flow⁴⁴ at these angles of yaw. Cross-flow separation at 4.5 degree yaw would not be expected because the lee side is still at a slight compressive angle to the free stream. When cross-flow separation occurs, there is a thickening of the boundary layer in the vicinity of the separation point (see Sketch). On the extreme lee side (near 180 degrees from the windward streamline) the boundary layer will be thinner; and hence, a higher heat-transfer rate will exist. This is the type of heat-transfer distribution observed at 9.5 and 13.7 degrees yaw. No schlieren pictures were taken to verify the existence of separated vortices because the model was yawed rather than pitched.



At each yaw angle, the free-stream Reynolds number was varied from approximately 2.5×10^5 to 2.2×10^6 per foot. In addition, data were taken at axial positions from 0.25 to 0.55 feet. Within the scatter of the data, there is apparently no effect of Reynolds number on the circumferential distributions for this range of test conditions.

As shown in Figure 10, there are four theoretical curves for each yaw angle. These curves have been calculated for the lowest and highest free-stream Reynolds numbers both with and without corrections for the

vortical layer. Second-order Stone theory¹⁵ as tabulated by Kopal¹⁸ has been used to determine the local flow conditions and the procedure developed by Willett²³ has been used to apply the second-order correction for the vortical layer. Laminar boundary-layer theory without interactions (Eq. (1)) is then applied using local flow conditions. This procedure essentially assumes local similarity and neglects cross-flow and pressure-gradient effects. Thus, there is little basis to expect that the method would be quantitatively accurate for a slender cone at large yaw. Surprisingly, the calculation is in reasonable agreement with the data on the windward side of the cone (up to ± 90 degrees from the most-windward streamline). On the lee side, the theoretical curves and the data do not agree, except at several fortuitous points. At the two largest yaw angles (9.5 and 13.7 degrees), the second-order Stone theory predicts negative pressures in the region 90 to 150 degrees from the most-windward streamline. The heat-transfer rate is assumed to be zero in this region. It is interesting that in the vicinity of the most-leeward streamline (180 ± 30 degrees), the theoretical curves follow the trend of the data fairly well for 9.5 degrees yaw. Such agreement should be considered fortuitous, since there is no justification for the theory in this region of separated flow. At 13.7 degrees, a similar agreement is not evident.

In comparing the theoretical curves with and without the vortical layer corrections, it is noted that the differences are not very large. Also, the curve without the correction lies below the curve with the vortical layer correction except in the neighborhood of the most-leeward

streamline at the two largest yaw angles. The accuracy of the theoretical method and the relatively small magnitude of the vortical layer corrections make it difficult to draw any conclusions from Figure 10 as to whether or not it is necessary to account for the existence of vortical layer in the present experiments.

BLUNT-NOSE CONE EXPERIMENTS AT ZERO YAW

For the blunt-nose experiments the cone was tested with flat noses having diameters of 0.0590, 0.1925, 0.2995, and 0.4000 inches. These produced a variation in length-to-nose diameter ratios from 1.75 to 112 at the instrumented stations, Table IV. The experimental heat-transfer rates are shown in Figure 11 and are compared with the zero-order ($\gamma=1$) blunt-cone theory of H. K. Cheng³². The correlation is made in terms of of the parameters

$$\frac{(\epsilon k)^{1/4} C_H \sqrt{Re_D}}{M_\infty \theta_c^2 \sqrt{C}} \quad \text{and} \quad \frac{\theta_c^2 X}{\sqrt{\epsilon k} D}$$

which appear in the zero-order theory. Note that the heat-transfer parameter, C_H , is based on free stream rather than local conditions.

In comparing the data with Cheng's theory, consideration must be given to the degree to which the experimental conditions match the theoretical assumptions. A comparison of these is given below

<u>Theoretical Assumption</u>	<u>Experimental Condition</u>
$\gamma \rightarrow 1$	$\gamma = 1.4$ (along cone)
$\epsilon = \frac{\gamma-1}{\gamma+1} \ll 1$	$\epsilon = 1/6$
$\frac{1}{2} \theta_s \frac{2(\gamma-1)}{\gamma} \ll 1$	$\frac{1}{2} \theta_s \frac{2(\gamma-1)}{\gamma} < \frac{1}{4}$ for $\frac{X}{D} > 3$
$M_\infty^2 \theta_s^2 \gg 1$	$M_\infty^2 \theta_s^2 > 4$ for all $\frac{X}{D}$

Thus if "small compared to unity" is taken as less than 1/4 and "large compared to unity" is taken as greater than 4, the conditions of the experiments reasonably meet the theoretical assumptions for X/D positions greater than 3.

Considering the zero-order nature of the theory³², the agreement shown in Figure 11 is reasonably good. The data initially decrease uniformly with increasing X/D, then show an increase similar to that indicated by the theory in the neighborhood of $\frac{\theta_c^2 X}{\sqrt{e k} D} = 1$, and subsequently decrease again. The data thus show qualitative verification of the undershoot and overshoot predicted by the theory. Also, the data establish this as an inviscid flow phenomenon since there is no pronounced Reynolds number effect apparent in the results. The oscillations in the theory occur at values of X/D greater than 100. Since the largest value of X/D obtained in the tests was 112, the existence of the oscillations could not be detected.

To further compare the experiments with theory, the shape of the shock wave was measured from schlieren photographs, Figure 12. The measured and theoretical shock shapes are shown in Figure 13. It is noted that the measured shock shapes are similar for all nose diameters. The bend in the theoretical curve represents the region where the influence of the cone makes itself felt on the shock. The data show a similar effect, though of a more gradual nature, occurring at X/D values of about 20 in contrast to the theoretical prediction of about 100. It is reasonable to expect the actual shock shape to display a more gradual change and the

change to occur nearer the nose, since the theory assumes an infinitely thin shock layer whereas in reality the shock layer has finite thickness.

In noting the difference in the absolute level of the data relative to theory, it should be indicated that the theory does not specify whether the distance from the body to the shock wave should be measured from the cone axis, the cone surface, or a distance $1/2 D$ from the cone axis.*

The experimental shock shapes have been measured from the cone axis. If the Y -dimension is measured from a distance $1/2 D$ from the cone axis, the data fall below the theoretical curve for small X/D , cross the curve at about $X/D = 3$, and lie above the theory at higher values of X/D . If the shock shape is measured from the cone surface, the data lie entirely below the theoretical curve, but closer to it than the data shown in Figure 13.

CONCLUSIONS

The present investigation of laminar heat transfer to a slender cone has included yaw, nose-bluntness, boundary-layer displacement and transverse-curvature effects; all phenomena that are likely to be experienced by a slender body in hypersonic flight. A cone model has the advantage that its geometry makes it amenable to theoretical analysis. The available theoretical solutions for the various flow phenomena involved have been reviewed, and the experimental data have been compared

* This ambiguity does not exist for the case of the flat plate, where the shock is clearly measured from the surface.

with predictions based on these theories. In some instances experiment and theory are in good agreement, whereas in other cases the disagreement is appreciable. The test flow conditions covered a free-stream Reynolds number range from about 2×10^5 to 2×10^6 per foot and a corresponding Mach number range from 11.3 to 13.0 in air. The test flow velocity was approximately 6500 ft/sec and the stagnation temperature about 2000°K .

From a comparison of the experimental results and the pertinent theoretical predictions, the following conclusions have been reached:

1. For the slender pointed cone at zero yaw the experimental data are in reasonably good agreement with both laminar boundary-layer theory and Eckert's empirical reference-enthalpy method when account is taken of the presence of boundary-layer displacement and transverse-curvature effects. However, as noted in the text, the variation of the data with Reynolds number for a given free-stream Reynolds number is slightly greater than the theoretical variation. Also, the allowance for boundary-layer displacement and transverse-curvature effects accounts for only about one-half of the discrepancy between the data and laminar boundary-layer theory at the highest free-stream Reynolds number. These discrepancies are believed to be related to the influence of the wake on the boundary layer on the model.
2. The agreement between the experimental data and theory including displacement and transverse curvature is best at the lowest free-stream Reynolds numbers. This indicates that no measurable slip-flow effects were present and agrees with Hayes and Probstein's

criterion for the slip-flow region rather than the criterion resulting from Tsien's analysis as described by Schaaf and Chambre.

3. The experimental heat-transfer data along the most-windward streamline are in good agreement with Reshotko's theoretical prediction at yaw angles up to 3 degrees and lies somewhat above the theory at higher yaw angles.
4. The yawed-cylinder theory of Reshotko and Beckwith has been calculated for yaw angles above 5 degrees and does not provide good agreement with the experimental data.
5. The experimental circumferential heat-transfer rates for large yaw angles (≥ 4.5 degrees) show fair agreement with an approximate theoretical calculation on the windward side of the cone. On the leeward side the agreement is poor except in certain fortuitous cases.
6. The experimental data suggest the presence of separated flow and trailing vortices on the lee side of a pointed 5-degree half-angle cone at 9.5- and 13.7-degree yaw.
7. The blunt-nose cone experiments indicate qualitative agreement of the measured heat-transfer rates and shock-wave shapes with the zero-order theory of H. K. Cheng.
8. The slender cone provides a useful means of determining flow angularity, when the position of the most-windward streamline is determined empirically from the circumferential heat-transfer distribution.

REFERENCES

1. Wittliff, C. E. and Wilson, M. R., Heat Transfer to Slender Cones in Hypersonic Air Flow Including Yaw and Nose-Bluntness Effects. IAS Preprint 61-213-1907. Paper presented at National IAS/ARS Joint Meeting, Los Angeles, Calif., June 13-16, 1961.
2. Taylor, G. I. and MacColl, J. W., The Air Pressure on a Cone Moving at High Speeds. Proc. Roy. Soc. London, Ser. A, Vol. 139, pp. 278-311, 1933.
3. Kopal, Z., Tables of Supersonic Flow Around a Cone. Tech. Rept. No. 1, Dept. of Elect. Eng., M. I. T., 1947.
4. Sims, J. L., Supersonic Flow Around Right Circular Cone Tables for Zero Angle of Attack. Rept. ABMA DA-TR-11-60, Army Ballistic Missile Agency, March 1, 1960.
5. Hayes, W. D. and Probstein, R. F., Hypersonic Flow Theory. Chap. VIII, pp. 284-325, Academic Press, New York, 1959.
6. Young, A. D., Modern Developments in Fluid Dynamics. High-Speed Flow. Vol. 1, Chap. X, Boundary Layers, Clarendon Press, Oxford, England, 1953.
7. Probstein, R. F., Interacting Hypersonic Laminar Boundary Layer Flow Over a Cone. Tech. Rept. AF2798/1, Brown Univ., March 1955.
8. Lees, L., Note on the Hypersonic Similarity Law for an Unyawed Cone. J. Aero. Sci., Vol. 18, No. 10, pp. 700-702, October 1951.

9. Mangler, W., Boundary Layers on Bodies of Revolution In Symmetrical Flow. Brit. Ministry of Aircraft Prod. Volkenrode Repts. and Trans. No. 55, 1946.
10. Probstein, R. F. and Elliot, D., The Transverse Curvature Effect in Compressible Axially Symmetric Laminar Boundary-Layer Flow. J. Aero. Sci., Vol. 23, No. 3, pp. 208-224, March 1956.
11. Schaaf, S. A. and Chambre, P. L., Flow of Rarefied Gases, in "Fundamentals of Gas Dynamics" (H. W. Emmons, Ed.), Sec. H, pp. 687-739 (Vol. III of "High Speed Aerodynamics and Jet Propulsion"), Princeton Univ. Press, Princeton, 1958.
12. Schaaf, S. A. and Talbot, L., Mechanics of Rarefied Gases, in Handbook of Supersonic Aerodynamics, Sec. 16, NAVORD Rept. 1488 (Vol. 5), February 1959.
13. Hayes, W. D. and Probstein, R. F., Ibid. Chap. X, pp. 375-383.
14. Stone, A. H., On Supersonic Flow Past a Slightly Yawing Cone. J. Math. and Phys., Vol. 27, pp. 67-81, 1948.
15. Stone, A. H., On Supersonic Flow Past a Slightly Yawing Cone II. J. Math. and Phys., Vol. 30, pp. 200-213, 1952.
16. Stone, A. H., Corrections to the Paper, "On Supersonic Flow Past a Slightly Yawing Cone II". J. Math. and Phys., Vol. 31, p. 300, 1953.
17. Kopal, Z., Tables of Supersonic Flow Around Yawing Cones. Tech. Rept. No. 3, Dept. Elect. Eng., M. I. T., 1947.
18. Kopal, Z., Tables of Supersonic Flow Around Cones of Large Yaw. Tech. Rept. No. 5, Dept. Elect. Eng., M. I. T., 1949.

19. Roberts, R. C. and Riley, J. D., A Guide to the Use of the M. I. T. Cone Tables. J. Aero. Sci., Vol. 21, No. 5, pp. 336-342, May 1954.
20. Sims, J. L., Supersonic Flow Around Right Circular Cones. Tables for Small Angle of Attack. Rept. ABMA DA-TR-19-60, Army Ballistic Missile Agency, April 27, 1960.
21. Ferri, A., Supersonic Flow Around Circular Cones at Angles of Attack. NACA Rept. 1045, 1951.
22. Cheng, H. K., Hypersonic Shock-Layer Theory of a Yawed Cone and Other Three-Dimensional Pointed Bodies. Cornell Aero. Lab. Rept. No. AF-1270-A-1, WADC TN 59-335, October 1959.
23. Willett, J. E., Vortical Layer Effects Around Circular Cones at Angles of Attack. Rept. No. 6765, Res. Dept., McDonnell Aircraft Corp., March 1959.
24. Moore, F. K.; Three-Dimensional Compressible Laminar Boundary-Layer Flow. NACA TN 2279, March 1951.
25. Moore, F. K., Laminar Boundary Layer on a Circular Cone in Supersonic Flow at a Small Angle of Attack. NACA TN 2521, October 1951.
26. Moore, F. K., Laminar Boundary Layer on a Cone in Supersonic Flow at Large Angle of Attack. NACA TN 2844, November 1952.
27. Reshotko, E., Laminar Boundary Layer with Heat Transfer on a Cone at Angle of Attack in a Supersonic Stream. NACA TN 4152, December 1957.
28. Brunk, W. E., Approximate Method for Calculation of Laminar Boundary Layer with Heat Transfer on a Cone at Large Angle of Attack in Supersonic Flow. NACA TN 4380, September 1958.

29. Reshotko, E. and Beckwith, I. E., Compressible Laminar Boundary Layer Over a Yawed Infinite Cylinder with Heat Transfer and Arbitrary Prandtl Number. NACA TN 3986, 1957.
30. Grimminger, G., Williams, E. P., and Young, G. B. W., Lift on Inclined Bodies of Revolution in Hypersonic Flow. J. Aero. Sci., Vol. 17, No. 11, pp. 675-690, November 1950.
31. Hayes, W. D. and Probstein, R. F., Ibid. Chap. III, Sec. 3.2, pp. 74-81; Chap. IV, Sec. 4.4, pp. 158-162, Chap. VI.
32. Cheng, H. K., Hypersonic Flow with Combined Leading-Edge Bluntness and Boundary-Layer Displacement Effect. Cornell Aero. Lab. Rept. No. AF-1285-A-4, August 1960.
33. Chernyi, G. G., Flow Past a Thin Blunt-Nosed Cone at High Supersonic Speed. RAE Library Translation No. 737, May 1958 (from Dokl. Akad. Nauk SSSR, 115 (1957) 4, pp. 681-683).
34. Lunev, V. V., Motion of a Slender Blunted Body in the Atmosphere with High Supersonic Speed. ARS Journal Supplement, Vol. 30, No. 4, pp. 414-415, April 1960.
35. Lees, L. and Kubota, T., Inviscid Hypersonic Flow Over Blunt-Nosed Slender Bodies. J. Aero. Sci., Vol. 24, No. 3, pp. 195-202, March 1957.
36. Wittliff, C. E., Wilson, M. R., and Hertzberg, A., The Tailored-Interface Hypersonic Shock Tunnel. Cornell Aero. Lab. Rept. No. AD-1052-A-8, AFOSR TN 59-31, AD 209203, January 1959; Also J. Aero/Space Sci., Vol. 26, No. 4, April 1959.

37. Wittliff, C. E. and Wilson, M. R., Nozzle Flow Study and Flow Angularity Measurements in the Hypersonic Shock Tunnel. Cornell Aero. Lab. Rept. No. AD-917-A-3, Part II, WADC TR 58-401, AD 207615, December 1958.

38. Cheng, H. K., Hall, J. G., Golian, T. C., and Hertzberg, A., Boundary-Layer Displacement and Leading-Edge Bluntness Effects in High-Temperature Hypersonic Flow. Cornell Aero. Lab. Rept. No. AD-1052-A-9, AFOSR TN 59-1193, January 1960; Also I. A. S. Paper No. 60-38, January 1960.

39. Vidal, R. J., Model Instrumentation Techniques for Heat Transfer and Force Measurements in a Hypersonic Shock Tunnel. Cornell Aero. Lab. Rept. No. AD-917-A-1, WADC TN 56-315, AD 97238, February 1956.

40. Wittliff, C. E. and Rudinger, G., Summary of Instrumentation Development and Aerodynamic Research in a Hypersonic Shock Tunnel. Cornell Aero. Lab. Rept. No. AD-917-A-2, Part I, WADC TR 58-401, AD 155758, August 1958.

41. Skinner, G. T., Analog Network to Convert Surface Temperature to Heat Flux. Cornell Aero. Lab. Rept. No. CAL-100, February 1960.

42. Hall, J. G. and Golian, T. C., Shock-Tunnel Studies of Hypersonic, Flat-Plate Airflows. Cornell Aero. Lab. Rept. No. AD-1052-A-10, AFOSR TR 60-142, December 1960.

43. Eckert, E. R. G., Survey on Heat Transfer at High Speeds. WADC TR 54-70, Univ. of Minn., April 1954.

44. Allen, H. J. and Perkins, E. W., Characteristics of Flow Over Inclined Bodies of Revolution. NACA RM A50L07, March 1951.

45. Hayes, W. D. and Probstein, R. F., *Ibid.* Chap. IX, pp. 333-353.
46. Talbot, L., Koga, T., and Sherman, P. M., Hypersonic Viscous Flow Over Slender Cones, NACA TN 4327, September 1958.
47. Probstein, R. F. and Bray, K. N. G., Hypersonic Similarity and the Tangent-Cone Approximation for Unyawed Bodies of Revolution, *J. Aero. Sci.*, Vol. 22, No. 1, pp. 66-68, January 1955.

APPENDIX A

BOUNDARY-LAYER DISPLACEMENT EFFECT ON CONES

A description of the viscous-inviscid interaction resulting from a thick boundary layer on a cone has been given in the text. A review of various theoretical analyses of this phenomenon may be found in Reference 45. For the conditions of the present experiments, the interaction is of the weak type studied by Probstein⁷ and Talbot, Koga, and Sherman⁴⁶ among others. The method of Reference 46 is a procedure for calculating only the self-induced pressures resulting from the viscous interaction, whereas Reference 7 treats not only the induced pressures but also the corrections to the skin friction and heat-transfer rate resulting from the interaction. In Reference 7, Probstein treats the "weak" interaction* wherein the governing parameter is of order unity. The present experiments covered the range $0.9 < \bar{x}_c < 4$, and the theory is generally applicable.

To determine the induced-pressure distribution, the pressure is expressed as a Taylor series expansion in powers of $d\delta^*/dx$

$$\frac{p}{p_c} = 1 + \frac{1}{p_c/p_\infty} \left[\frac{d(p/p_\infty)}{d\theta} \right]_{\theta=\theta_c} \left(\frac{d\delta^*}{dx} \right) + \frac{1}{2!} \frac{1}{p_c/p_\infty} \left[\frac{d^2(p/p_\infty)}{d\theta^2} \right]_{\theta=\theta_c} \left(\frac{d\delta^*}{dx} \right)^2 + \dots \quad (A-1)$$

where the total flow deflection angle, θ , is given by $\theta = \theta_c + d\delta^*/dx$ and p_c is the pressure on a cone of angle θ_c in the absence of boundary-layer

* The "strong" interaction exists only in a region near the nose. There was no heat-transfer instrumentation located in this region during the present experiments.

displacement effects. The tangent-cone approximation⁴⁷ is applied and the coefficients of $d\delta^*/dx$ are evaluated numerically using Lees' hypersonic approximation⁸ for $K = M_\infty \theta_c \geq 1$.

The rate of growth of the boundary-layer displacement thickness is taken to be

$$\frac{d\delta^*}{dx} = d_c M_\infty^2 \sqrt{C_c} / \sqrt{3 R e x_c} \quad (A-2)$$

where

$$d_c = \frac{A}{M_c^2} \frac{T_w}{T_c} + B(\gamma - 1) \quad (A-3)$$

and $A = 0.865$, $B = 0.166$ for $\text{Pr} = 1$

or $A = 0.968$, $B = 0.145$ for $\text{Pr} = 0.725$

The general expression for the induced pressure becomes

$$\frac{P}{P_c} = 1 + F_1(K) d_c \bar{x}_c + F_2(K) d_c^2 \bar{x}_c^2 \quad (A-4)$$

where $F_1(K)$ and $F_2(K)$ are functions of the hypersonic similarity parameter, K , and the specific heat ratio, γ , and are plotted in Reference 7 for $\gamma = 1.40$ and 1.66 .

Talbot, Koga and Sherman have shown⁴⁶ that Probstein's method is less accurate than their numerical graphical procedure in predicting the induced pressures when $K < 1$. This is to be expected since the hypersonic similarity approximation becomes invalid for $K < 1$. For the present experiments, the lowest value of the hypersonic similarity parameter is $K = 0.986$, but Probstein's procedure has been used in order

to be consistent with his result for the effect of boundary-layer displacement on heat transfer.

To obtain the effect of the induced pressures on the boundary-layer characteristics, the velocity and temperature in the boundary layer are expanded as follows

$$u = u_0(\eta) + u_1(\eta) \bar{x}_c + \dots + u_m(\eta) \bar{x}_c^m \quad (A-5)$$

$$T = T_0(\eta) + T_1(\eta) \bar{x}_c + \dots + T_m(\eta) \bar{x}_c^m \quad (A-6)$$

where η is the compressible "similarity" parameter proportional to y/\sqrt{x} . These expansions are introduced into the laminar boundary-layer equations. Probstein⁷ states that Elliot and he, in an unpublished analysis, have computed numerical solutions with $\text{Pr} = 1$ for the first-order corrections to the velocity and temperature distributions. These have been used to obtain the first-order correction to the heat transfer

$$\frac{g - g_0}{g_0} = \left[-0.350 + 0.111 \frac{T_w}{T_c} + (0.429\gamma - 0.028) M_c^2 \right] \frac{d_c F_1(K) \bar{x}_c}{\gamma M_c^2} \quad (A-7)$$

APPENDIX B

DETERMINATION OF FLOW ANGULARITY FROM CIRCUMFERENTIAL HEAT TRANSFER DISTRIBUTIONS

The heat-transfer distribution around a sharp, slender cone is sensitive to the inclination of the model to the flow. Thus, when the 5° half-angle cone was tested at zero yaw relative to the nozzle centerline, the heat transfer around the cone varied by as much as 60% because of flow angularity. Previously, heat-transfer-instrumented wedges has been used to measure the flow angularity in the test section of the present nozzle³⁷. Those measurements indicated a "source-like" angularity of about 1/2° to 1° in the horizontal plane of symmetry. An analysis of the heat-transfer distribution for the present experiments has produced additional information concerning the flow angularity. In general, this information confirms the earlier flow measurements using the wedges.

Inspection of the experimental heat-transfer distributions for the zero-geometrical-yaw tests indicated that the variation had a "sine-like" nature. This is in agreement with expected variations in the inviscid flow field for small yaw angles. The heat-transfer rate is proportional to the square root of the product of the density and velocity and will have a harmonic circumferential variation to first order. For example,

$$q = St \rho U (H_{aw} - H_w) \quad (B1)$$

and

$$St = 0.675 R_e^{-1/2} \quad (B2)$$

Neglecting the circumferential variations of $(H_{aw} - H_w)$ and viscosity, one can write

$$g \sim \sqrt{\rho U} \quad (B3)$$

where, according to first-order theory¹⁴

$$U = \bar{U} + \alpha U_1 \cos \omega \quad (B4)$$

$$\rho = \bar{\rho} + \alpha \rho_1 \cos \omega \quad (B5)$$

and the bars denote the zero-yaw quantities. To first order, there results

$$\begin{aligned} \sqrt{\rho U} &= \sqrt{\bar{\rho} \bar{U}} \left[1 + \left(\frac{\alpha U_1}{\bar{U}} + \frac{\alpha \rho_1}{\bar{\rho}} \right) \cos \omega \right]^{1/2} \\ &= \sqrt{\bar{\rho} \bar{U}} \left[1 + \frac{1}{2} \left(\frac{\alpha U_1}{\bar{U}} + \frac{\alpha \rho_1}{\bar{\rho}} \right) \cos \omega + \dots \right]. \end{aligned} \quad (B6)$$

or

$$g \sim \sqrt{\rho U} \sim \sqrt{\bar{\rho} \bar{U}} \left[1 + \text{constant} \times \cos \omega \right] \quad (B7)$$

On this basis sine curves have been fitted to the experimental data by a least-squares technique for runs at 0° , $\pm 1^\circ$, and $\pm 2^\circ$ geometrical yaw, for example, see Figure 14. The position of maximum heat-transfer rate is the most-windward or stagnation streamline in the plane of the flow angularity. This can be related to the pitch and yaw components of the flow angularity as follows

$$\tan \omega_{g_{\max}} = \frac{\tan \alpha}{\tan(\beta + \psi)} \quad (B8)$$

where

$\omega_{g_{max}}$ = the circumferential position of the most-windward stream-line,

α, β = pitch and yaw components of the flow angularity,

ψ = geometrical yaw of the cone in the tunnel (geometrical pitch = 0).

Since there are two unknowns in this equation, it is necessary to take the runs by pairs to obtain a solution. With the exception of one of these runs at zero yaw, all of the runs gave consistent values of $\alpha = -0.8^\circ$ and $\beta = -0.6^\circ$ when all possible combinations were used. These values are in reasonably good agreement with the wedge-rake results. The net angularity is -1° in a plane rotated 35° clockwise (looking upstream) from the vertical. In other words, to have the model at a true zero inclination to the flow it would have to be set nose up 0.8° and to the right (looking upstream) 0.6° .

The pitch component of the angularity may be produced by the flow-turning wedge located between the primary and terminal nozzle expansions. A calculation of the boundary-layer growth on this flat plate indicates an approximate value of $d\delta/dx$ of 0.02 or an inclination of 1.2° . The corresponding value of $d\delta^*/dx$ is 0.006. These values are sufficiently close to the measured pitch angularity to believe that the boundary layer on the flow-turning wedge is the cause of this angularity. In future experiments this can be eliminated by adjusting the angle of the flow-turning wedge.

No definite cause for the yaw angularity of 0.6° has been determined. It may be a local disturbance from a sidewall irregularity or a lateral misalignment in the various stages of the nozzle.

TABLE I
FLOW CONDITIONS FOR POINTED CONE ZERO YAW TESTS

Run No.	Yaw Angle	Stagnation Pressure (psia)	Stagnation Temperature (°K)	Re/ft
522	0°	9,731	1989	17.4 x 10 ⁵
523	0°	4,500	1989	9.0 "
524	0°	920	1939	2.4 "

TABLE II
FLOW CONDITIONS FOR YAWED POINTED CONE TESTS

Run No.	Yaw Angle	Stagnation Pressure (psia)	Stagnation Temperature (°K)	Re/ft
525	- 1°	4,190	1948	9.6 x 10 ⁵
526	- 2°	4,190	1968	9.3 "
527	+ 1°	4,203	1892	10.4 "
528	+ 2°	4,200	1982	9.2 "
529	+ 5°	4,220	2024	8.8 "
530	+ 5°	1,050	1996	2.3 "
531	+ 5°	11,150	1989	24.4 "
532	+10°	10,325	2018	21.8 "
533	+10°	4,588	1954	10.4 "
534	+10°	1,044	1883	2.6 "
535	+14°16'	1,120	1863	2.8 "
536	+14°16'	4,567	1954	10.4 "
537	+14°16'	8,950	1968	20.0 "

TABLE III
FLOW CONDITIONS FOR BLUNTED CONE ZERO YAW TESTS

Run No.	D _{Nose} (inches)	Stagnation Pressure (psia)	Stagnation Temperature (°K)	Re/L (ft ⁻¹)
721	.1925	9,608	1932	1.537 x 10 ⁶
722	"	10,323	2016	1.542 x 10 ⁶
723	"	5,432	2079	8.142 x 10 ⁵
724	"	5,252	2037	8.277 x 10 ⁵
725	"	1,465	1980	3.190 x 10 ⁵
726	"	1,438	1959	3.208 x 10 ⁵
727	.2995	10,503	2037	1.498 x 10 ⁶
728	"	10,188	2001	1.508 x 10 ⁶
729	"	5,490	2094	8.104 x 10 ⁵
730	"	5,319	2058	8.164 x 10 ⁵
731	"	1,448	1971	3.207 x 10 ⁵
732	"	1,438	1959	3.208 x 10 ⁵
733	.400	10,143	1995	1.505 x 10 ⁶
734	"	10,188	2001	1.508 x 10 ⁶
735	"	4,804	1932	8.630 x 10 ⁵
736	"	5,396	2070	8.186 x 10 ⁵
737	"	1,536	2037	3.125 x 10 ⁵
738	"	1,483	1995	3.155 x 10 ⁵
50	.059	610	2069	1.414 x 10 ⁵
51	"	610	2069	1.387 x 10 ⁵
54	"	4,376	1830	8.523 x 10 ⁵
55	"	4,501	1859	9.656 x 10 ⁵
56	"	8,840	1898	1.554 x 10 ⁶

TABLE IV
**X/D POSITIONS OF INSTRUMENTED STATIONS FOR
BLUNTED CONES**

	Station A	Station B	Station C
D = 0.0590"	50.8	86.6	111.8
D = .1925"	9.8	20.5	28.5
D = .2995"	4.30	11.2	16.25
D = .400"	1.75	7.0	10.75

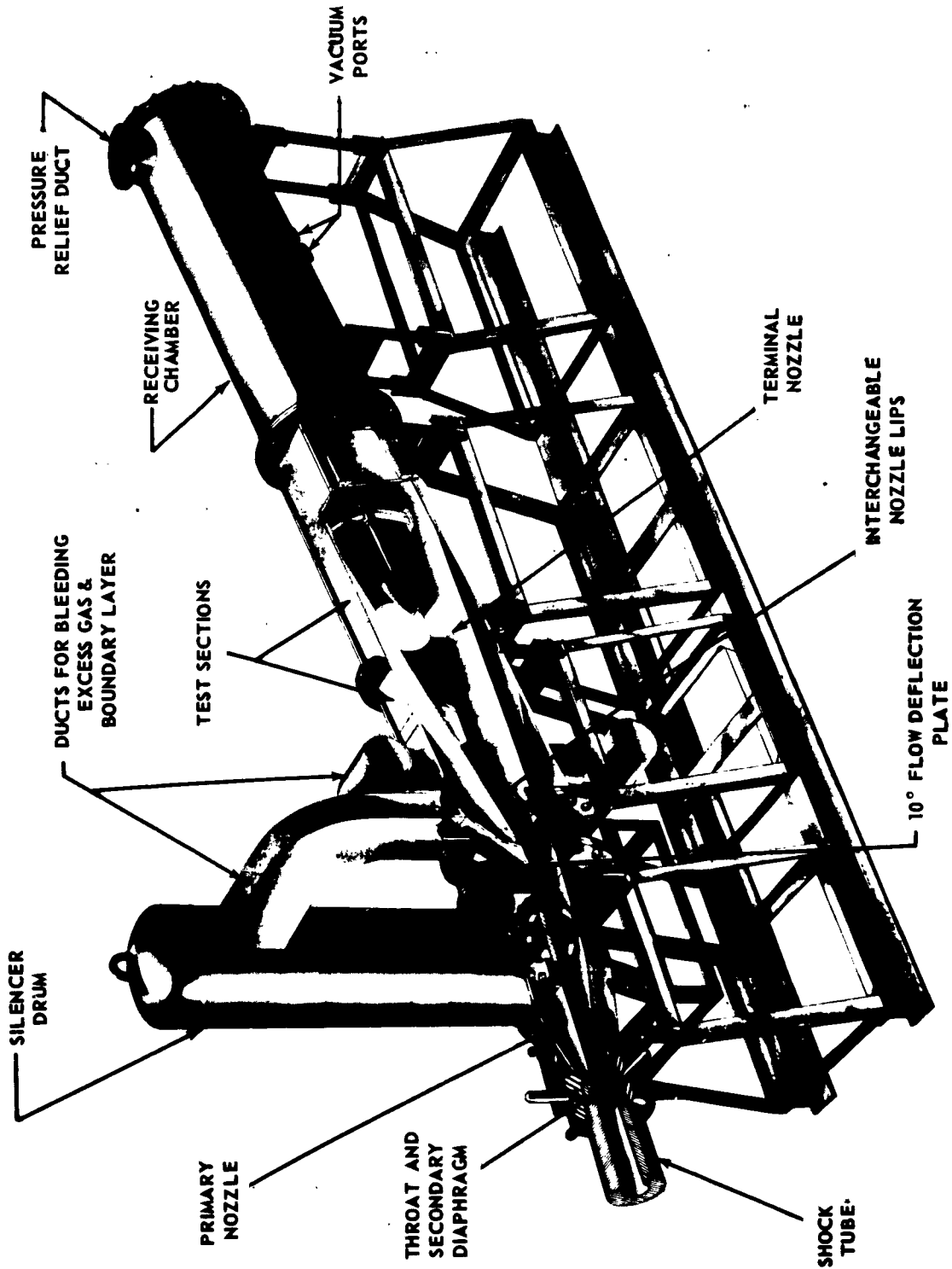


Figure 1 CORNELL AERONAUTICAL LABORATORY 11 INCH BY 15 INCH HYPERSONIC SHOCK TUNNEL

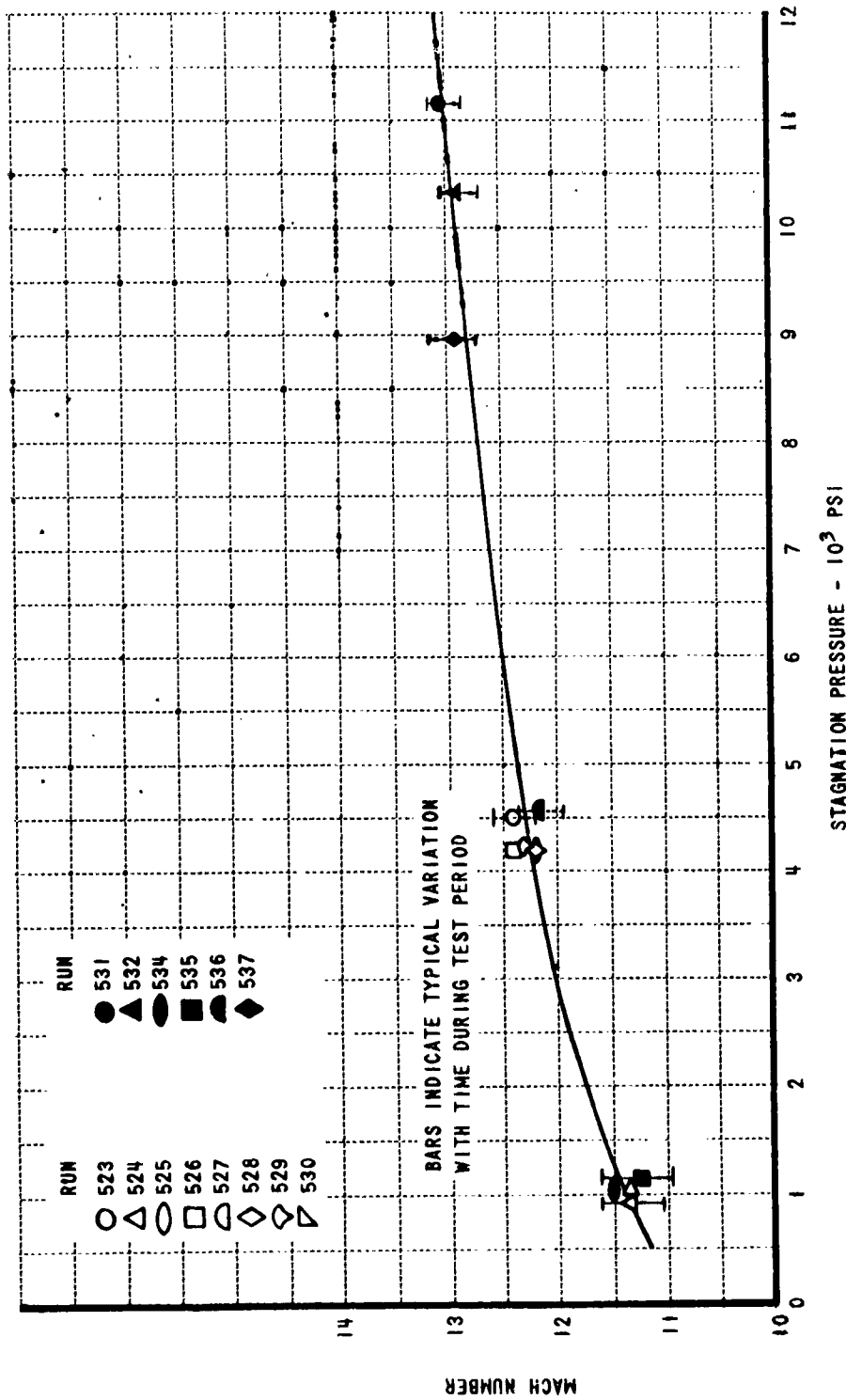


Figure 2 VARIATION OF MACH NUMBER WITH NOZZLE STAGNATION PRESSURE

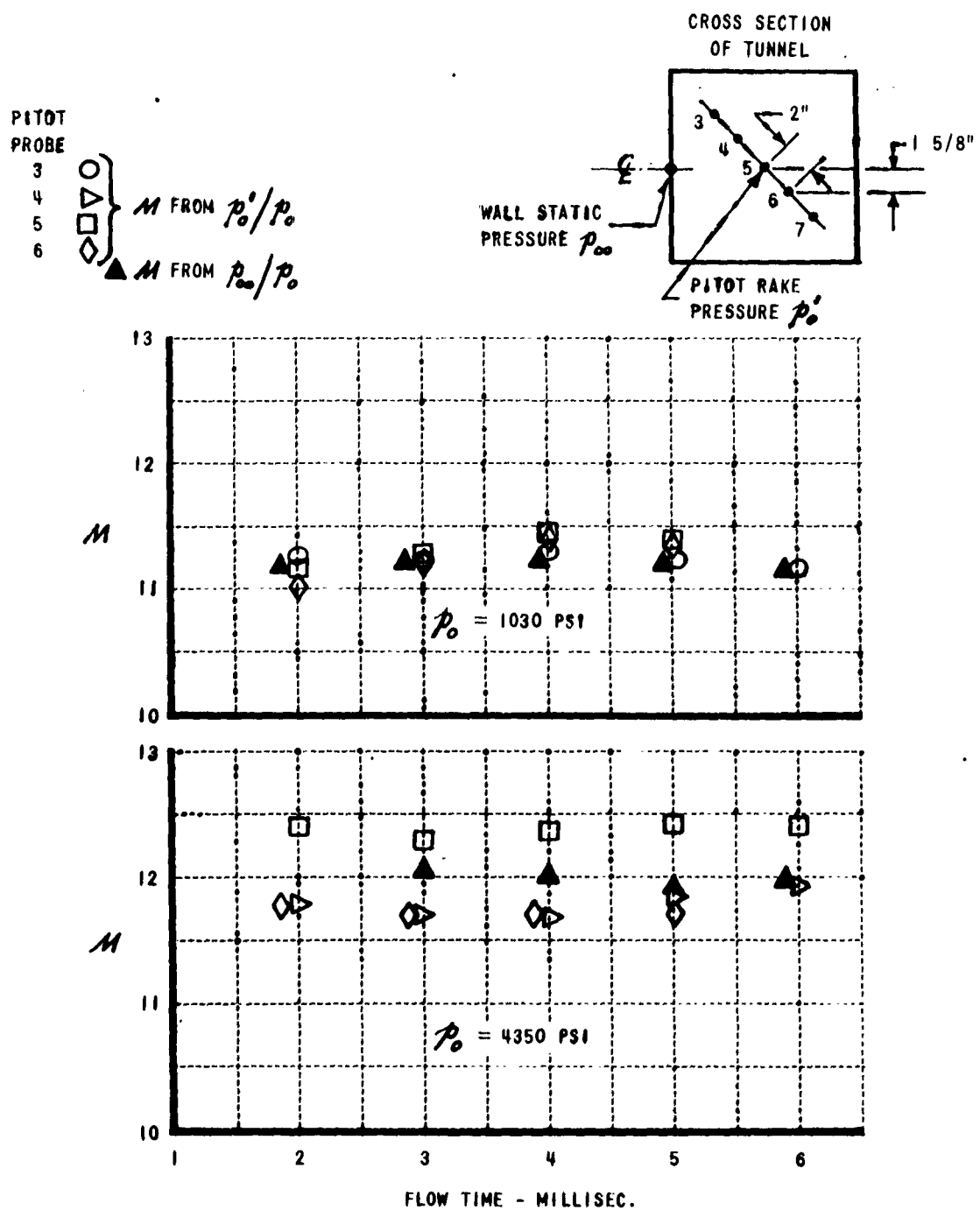


Figure 3 TYPICAL CALIBRATION RESULTS FOR MACH NUMBER (M) SURVEY

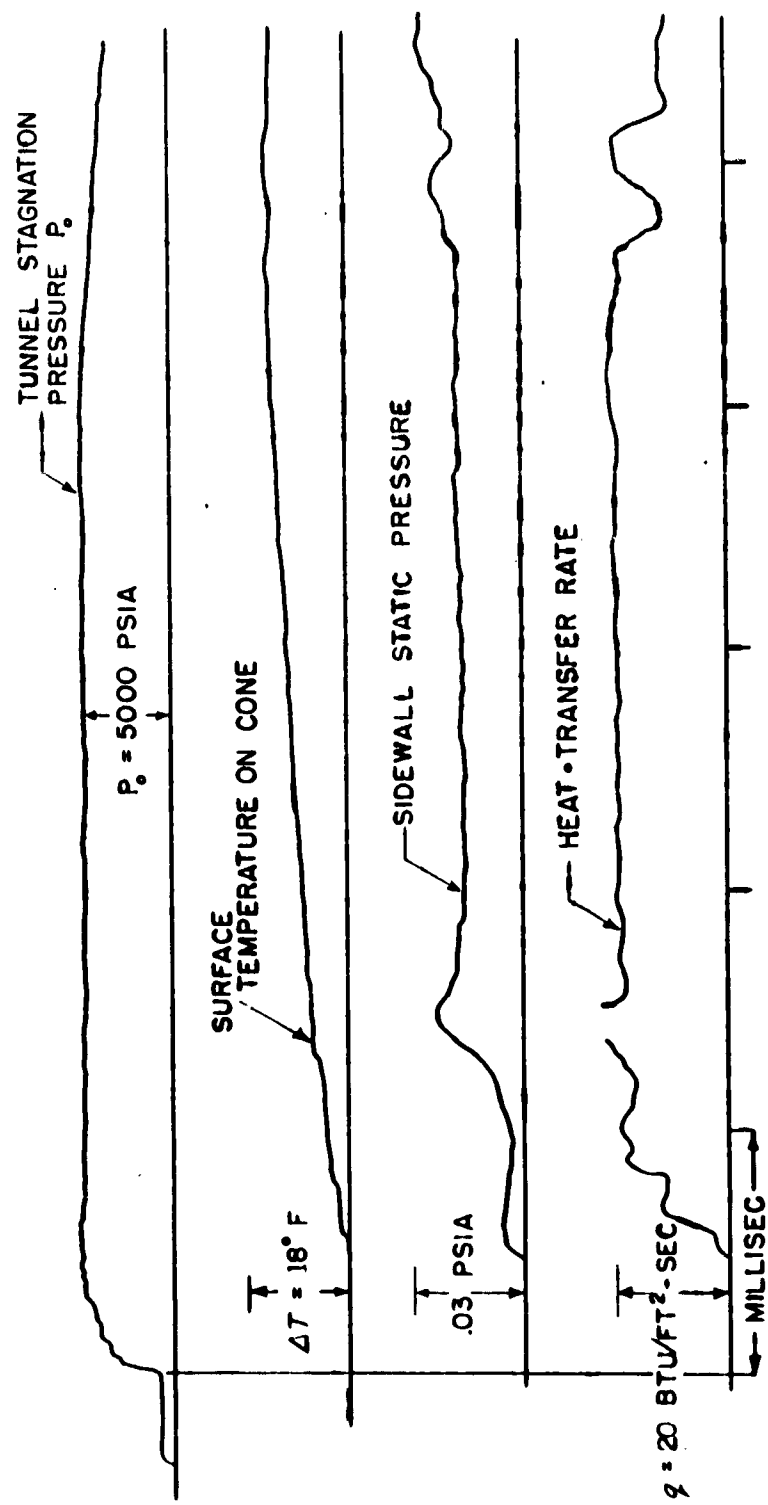


Figure 4 TYPICAL DRUM - CAMERA OSCILLOSCOPE RECORD



Figure 5a PHOTOGRAPH OF SHARP 5° HALF-ANGLE CONE

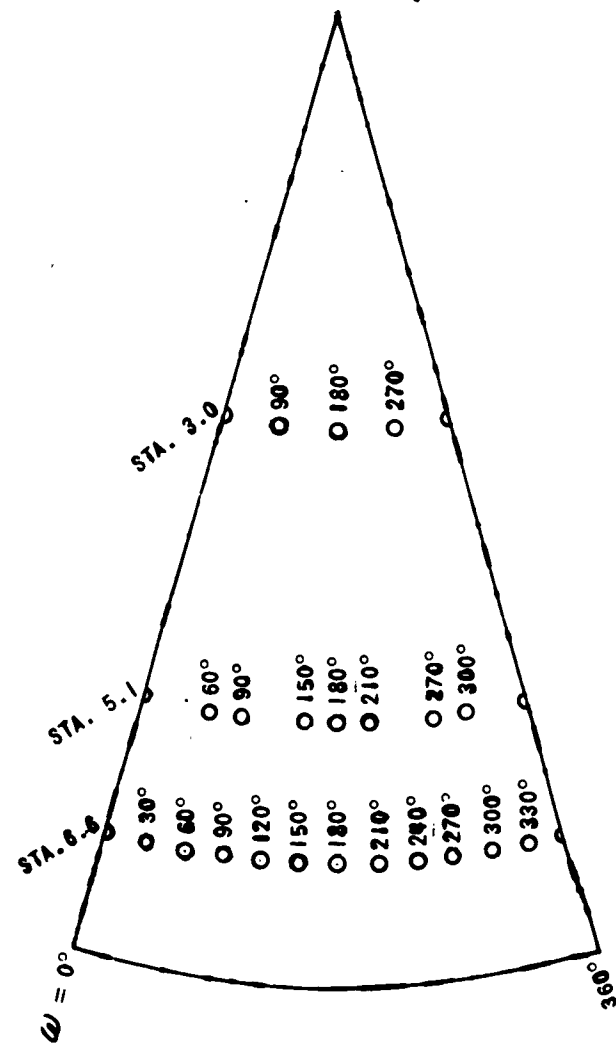
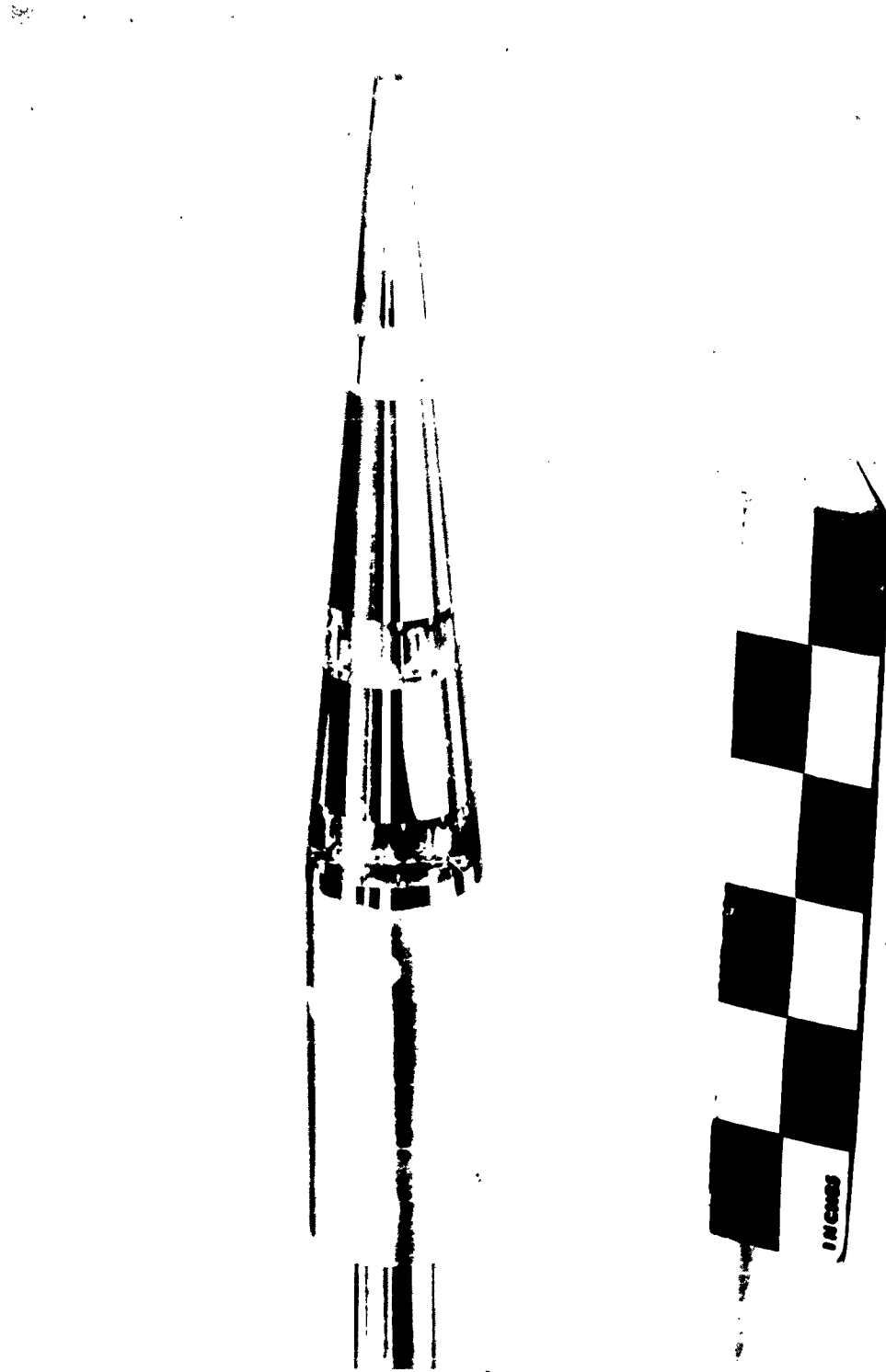


Figure 5b SKETCH OF 5° HALF-ANGLE CONE SHOWING LOCATION OF HEAT TRANSFER ELEMENTS

Figure 6 BLUNTED CONE MODEL, $D = .1925$ INCHES



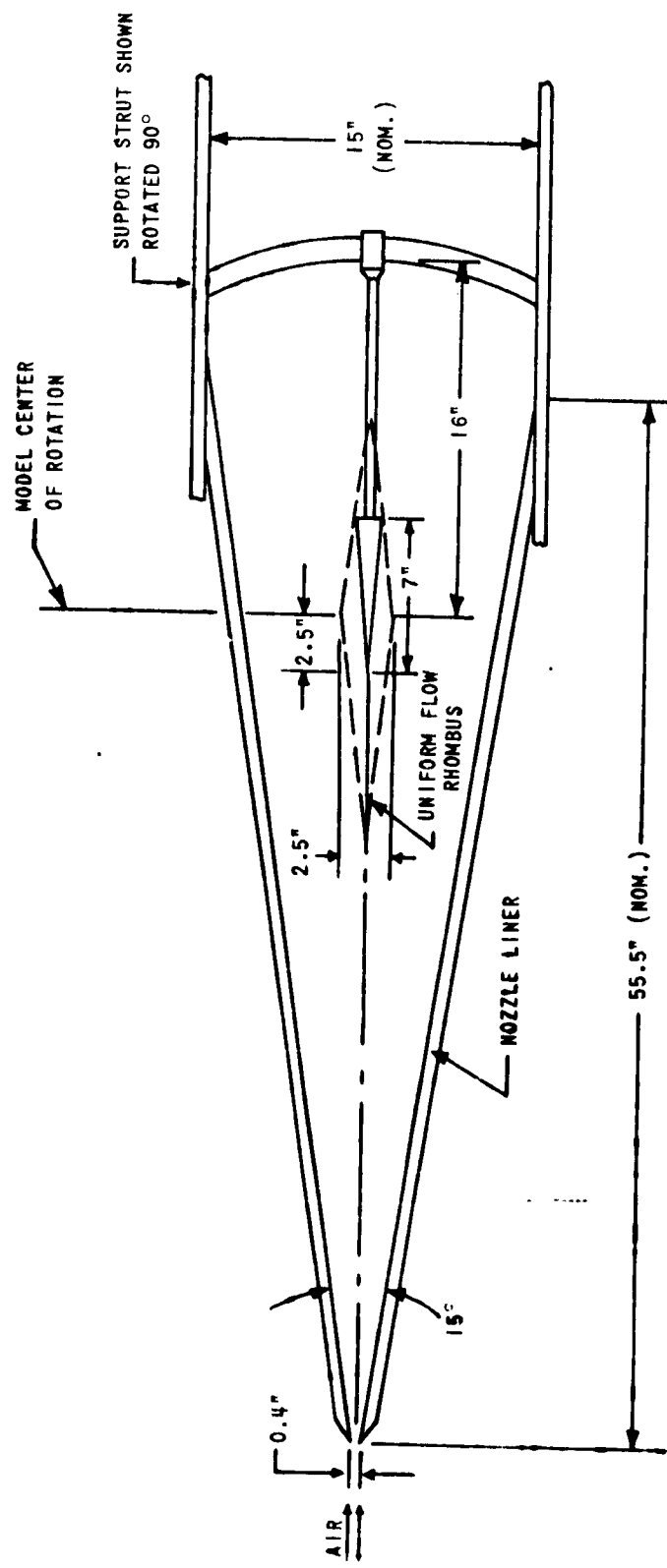


Figure 7 15° WEDGE NOZZLE USED FOR TESTS

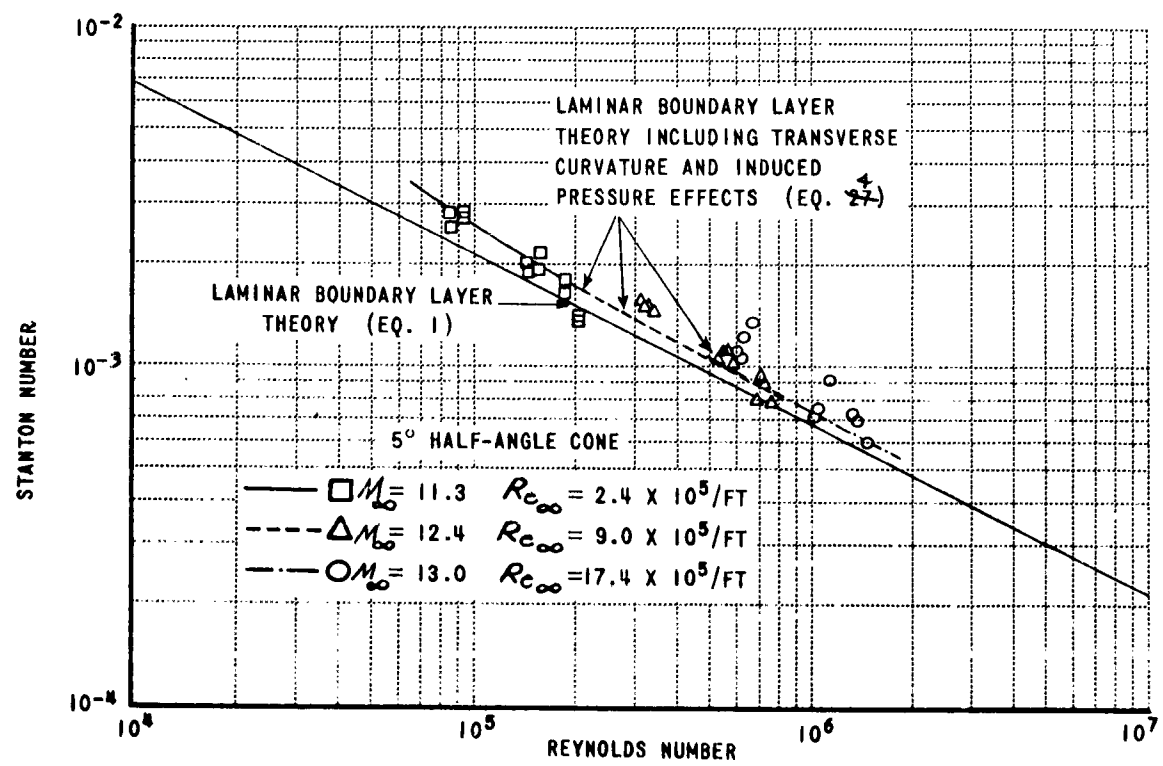


Figure 8 HEAT TRANSFER TO A POINTED CONE AT ZERO YAW COMPARED WITH LAMINAR THEORY

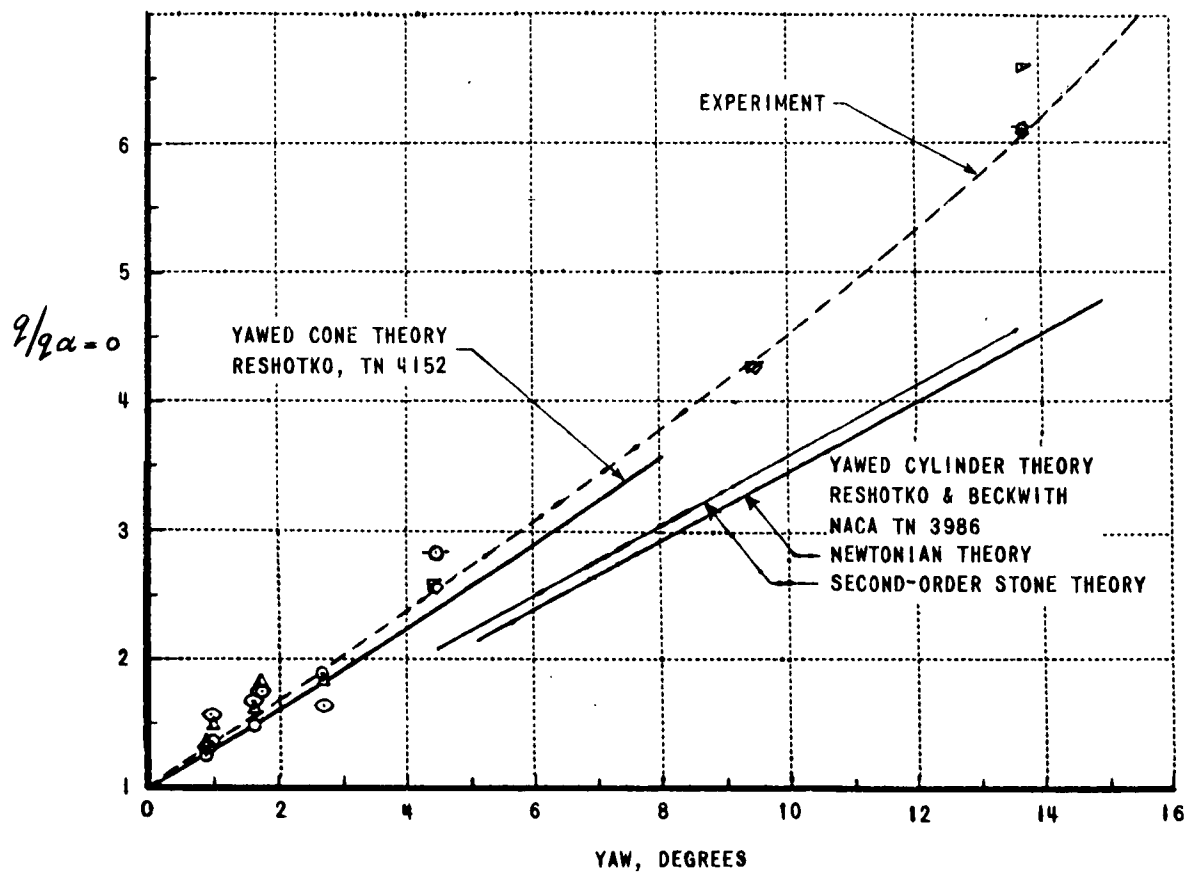


Figure 9 RATIO OF HEAT TRANSFER ALONG MOST WINDWARD STREAMLINE TO ZERO YAW HEAT TRANSFER - 5° HALF-ANGLE CONE AT $M = 12$, $T_{STAG} = 2000^\circ K$

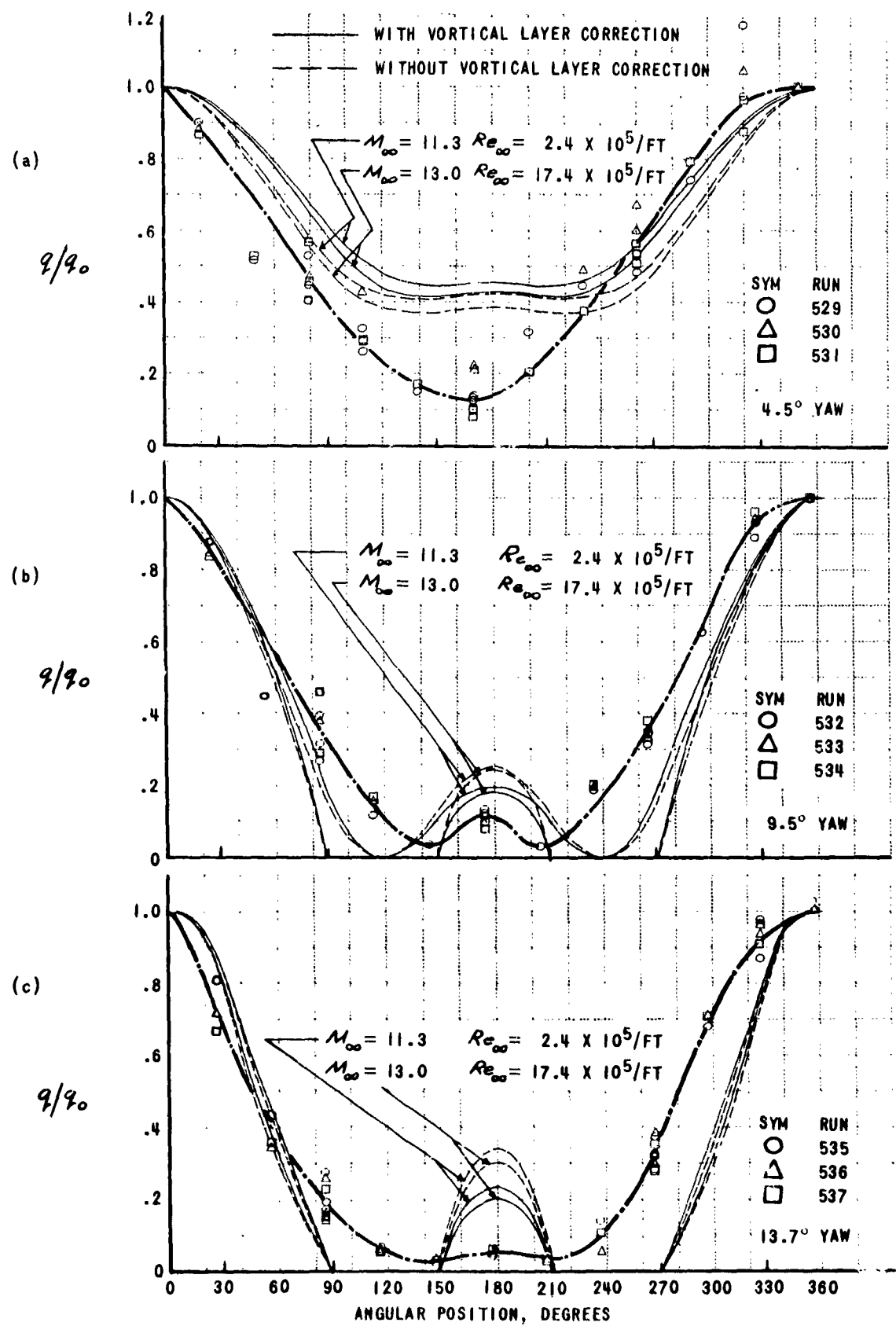


Figure 10 CIRCUMFERENTIAL HEAT TRANSFER DISTRIBUTION

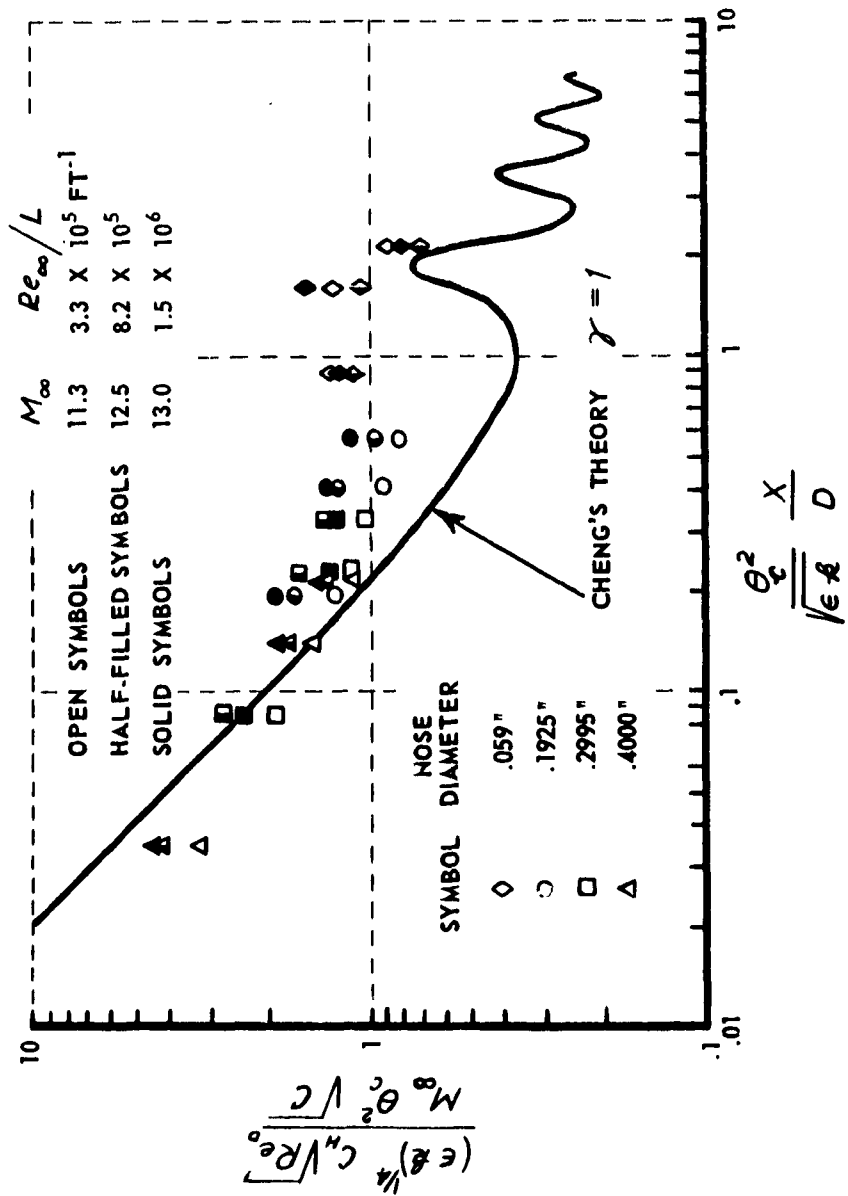


Figure 11 HEAT TRANSFER TO A BLUNT 5° HALF-ANGLE CONE AT ZERO YAW



Figure 12 SCHLIEREN PICTURE OF BLUNTED CONE, $D = .1925$ INCHES

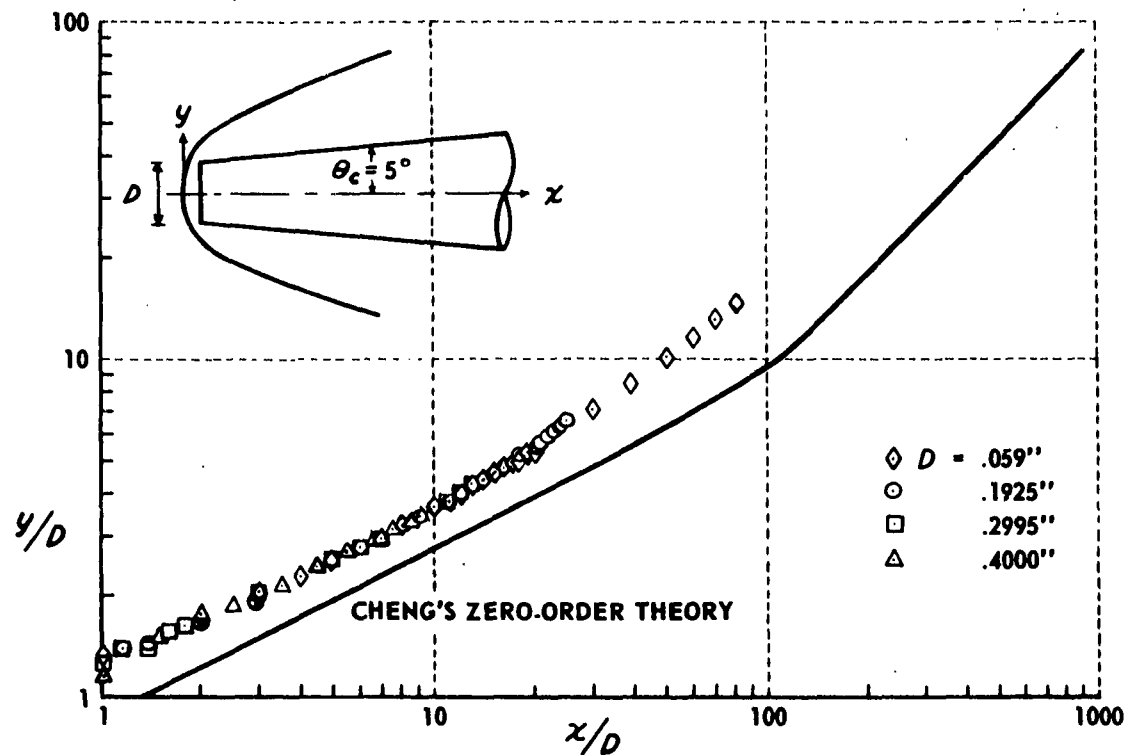


Figure 13 SHOCK WAVE SHAPE FOR A BLUNT 5° HALF-ANGLE CONE AT ZERO YAW

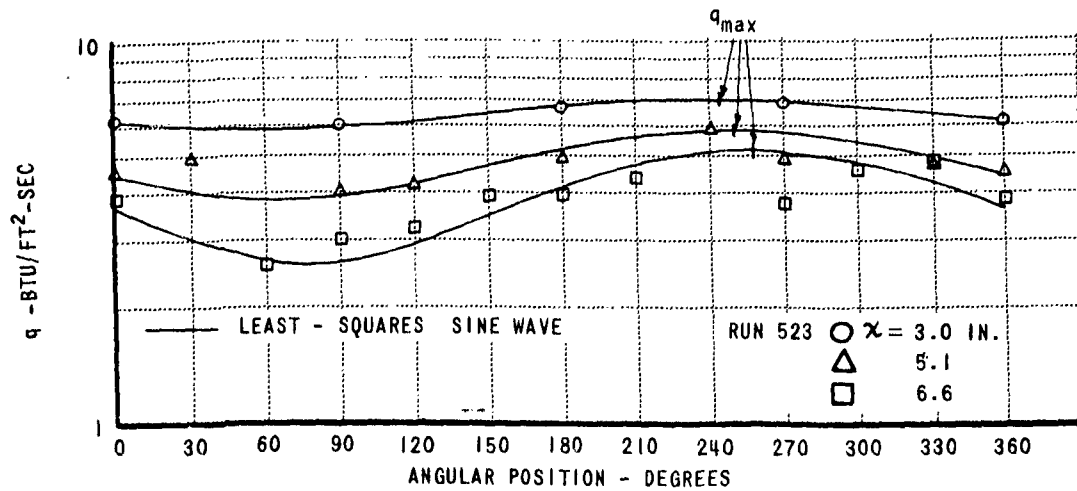


Figure 14a CIRCUMFERENTIAL HEAT TRANSFER DISTRIBUTION - RUN 523

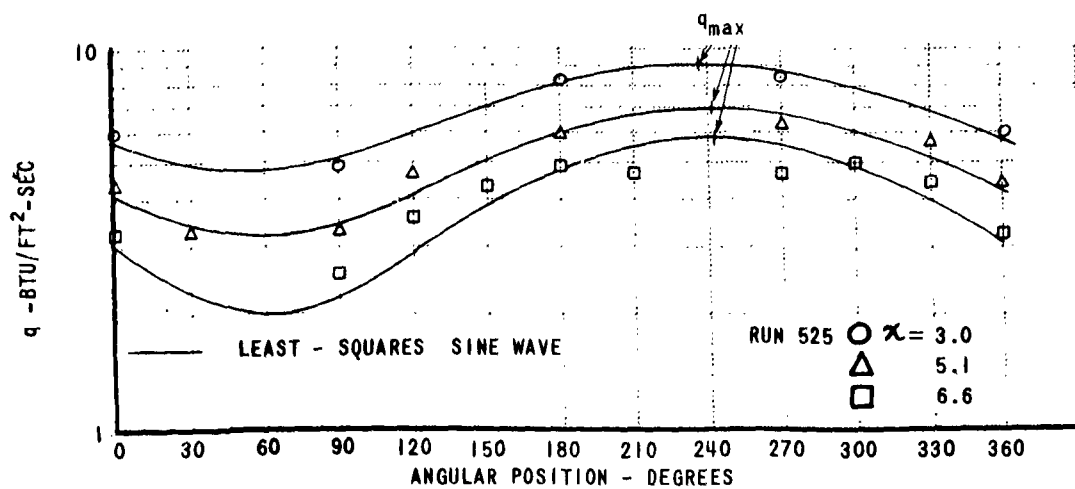


Figure 14b CIRCUMFERENTIAL HEAT TRANSFER DISTRIBUTION - RUN 525

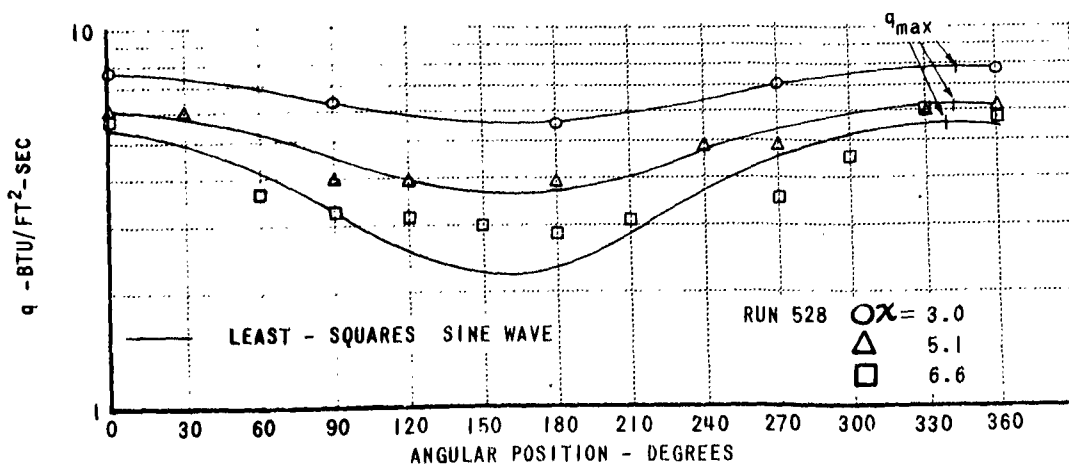


Figure 14c CIRCUMFERENTIAL HEAT TRANSFER DISTRIBUTION - RUN 528